CHALMERS UNIVERSITY OF TECHNOLOGY

NUMERICAL SIMULATION OF TURBULENT FLOW IN VENTILATED ROOMS

by

Lars Davidson

Submitted to the School of Mechanical Engineering
Chalmers University of Technology in partial
fulfillment of the requirements for the degree
of Doctor of Philosophy

Opponent: Dr. R. Holmberg, Fläkt AB, Jönköping, Sweden

Department of Applied Thermodynamics and Fluid Mechanics
Chalmers University of Technology
S-412 96 Göteborg , Sweden

Göteborg, April 1989

This thesis is based on the work contained in the following papers:

I. DAVIDSON, L. and OLSSON, E., " Calculation of Age and Local Purging Flow Rate in Rooms", Bldg. Environ., Vol. 22, pp. 111-127, 1987.

II. DAVIDSON, L. and OLSSON, E., "Calculation of some Parabolic and Elliptic Flows Using a New One-Equation Turbulence Model", Proceedings of 5th International Conference on Numerical Methods in Laminar and Turbulent Flow, Montreal, Vol. 1, pp. 411-422, 1987.

III. DAVIDSON, L. and HEDBERG, P., "Mathematical Derivation of a Finite-Volume Formulation for Laminar Flow in Complex Geometries", International Journal of Numerical Methods in Fluids, Vol. 9, pp. 531-540, 1989.

IV. DAVIDSON, L., HEDBERG, P. and OLSSON, E., "A Finite-Volume Computer Program for Turbulent Flow in Complex Geometries", Proceedings of 7th International Conference on Finite Element Methods in Fluid Problems, Huntsville, Alabama, pp. 390-395, 1989.

V. DAVIDSON, L., "Ventilation by Displacement in a Three-Dimensional Room: A Numerical Study", accepted for publication in Building and Environment, March, 1989.

VI. DAVIDSON, L., "Calculation of the Turbulent Buoyancy-Driven Flow in a Rectangular Cavity Using an Efficient Solver and Two Different Low Reynolds Number k-ϵ Turbulence Models", Rept., Dept. of Applied Thermodynamics and Fluid Mechanics, Chalmers University, of Technology, Göteborg, 1989.

CONTENTS

page

Abstract 4

Acknowledgments 6

Nomenclature 7

1. Introduction 11

2. Computation Method 12
   2.1 Different Differencing Schemes 14
   2.2 Solving the Discretized Equations 15
   2.3 The k-ε Turbulence Model 16
   2.4 The Wall Functions 17

3. Summary of papers 20
   3.1 Paper I 20
   3.2 Paper II 27
   3.3 Papers III and IV 31
   3.4 Paper V 37
   3.5 Paper VI 43

4. Concluding Remarks 55

References 57

ABSTRACT

A new one-equation turbulence model has been developed and tested. The turbulent viscosity is obtained as the product of the squareroot of the turbulent kinetic energy and the turbulent length scale. The turbulent length scale is obtained from an equation, which is based on an analogy of von Karman's equation, and involves the turbulent kinetic energy and the normal distance from the (nearest) wall. The model is tested in three parabolic flows and four elliptical flows. The CPU time was reduced by up to a factor two compared with the k-ϵ model.

The local purging flow rate and the local age in ventilated rooms are numerically investigated. The local age at a point is the time that has elapsed since the air, passing this point, entered the room. The local purging flow rate at a control volume P is the local net flow rate that is supplied to P.

A computer code for complex geometries, written for general nonorthogonal coordinates, has been developed including a k-ϵ turbulence model. When the velocity component, v_{1e} (or v_{2n}, see Fig. 3.7), is solved, the neighbouring velocities are projected in the direction of the velocity component v_{1e} (or v_{2n}). Thus we change the base vectors at the neighbouring points.

When using upwind differencing, the use of projected velocities gives better results than when curvature effects are included in the source term. The code is applied to two laminar and two turbulent flows: the calculated results are compared with experimental data.

The flow in a displacement flow system is numerically simulated. In these systems cool air is supplied near the floor at low velocity (see Fig. 3.12) which is heated by persons and/or machinery in the room. The flow in the room is divided into two zones: a lower zone (the occupied zone) to which clean cool air continuously is supplied, and an upper zone (above the occupied zone) where contaminated warm air is recirculating.

The buoyancy driven flow in a tall rectangular cavity of 5:1 aspect ratio with a Rayleigh number of $4 \cdot 10^{10}$ is calculated. The CELS solver is compared

with SIMPLEC, and it is shown to be up to more than three times as fast as SIMPLEC.

A modified form of a low Reynolds number k-ϵ turbulence model is developed. This model may have the capacity to handle free flow low Reynolds number effects. The model is, furthermore, consistent in its near-wall behaviour, and it allows simulation of the decay of grid turbulence. The model of Lam and Bremhorst (1981) is also tested. Both turbulence models predict transition and relaminarization regions according to experiments.

Keywords: one-equation turbulence model, ventilation parameter, general curvilinear coordinates, curvature effects, projected velocities, ventilation by displacement, low Reynolds number, transition, relaminarization, CELS solver

ACKNOWLEDGEMENTS

This work has been carried out at the Department of Applied Thermodynamics and Fluid Mechanics, Chalmers University of Technology, under the supervision of Professor Erik Olsson. The Swedish Council for Building Research has sponsored this work.

I would like to thank Erik Olsson for his support of me during the work. I would also like to thank Peter Hedberg with whom I carried out the work in Papers III and IV, and Dr. Mats Sandberg at the National Swedish Institute for Building Research, who initiated the work on ventilation parameters.

As mentioned, the work presented in Papers III and IV has been carried out together with Peter Hedberg. The development of the computer code used in these papers, as well as setting up the test cases, was carried out by both authors. However, the mathematical derivation in Paper III was carried out by myself.

NOMENCLATURE

A	area
B	width of room
c	concentration of contaminant
c_0	initial concentration
$c_{\epsilon 1}, c_{\epsilon 2}, c_D, c_\mu, c'_\mu$	constants in turbulence models
f_1, f_2, f_μ	damping functions in the turbulence model
g	acceleration due to gravity
g_{ij}, g^{ij}	metric tensor (covariant and contravariant components)
$\vec{g}_i$	unit base vector
H	height of room
k	turbulent kinetic energy
L	length of room
L_t	turbulent length scale
ℓ	characteristic turbulent length scale
$\dot{m}$	mass flow rate
n	coordinate in the normal direction from the wall
$\vec{n}$	normal vector
p	pressure

P_k	turbulence generating source term in the k and ϵ-equations
Q	total mass (volume) flow rate, or heat source
q	local heat transfer rate at the vertical walls per unit area [kW/m^2]
R_n	local Reynolds number ($=\rho\sqrt{k}\ n/\mu$)
R_t	local Reynolds number [$=\rho k^2/(\mu\epsilon) \sim \sqrt{k}\ \ell/\nu$]
r	constant factor when computing flow rate (section 3.4)
S^ϕ	source term of general variable
T	temperature in ^oK
t	temperature in ^oC
U, V, W	mean velocity in x, y and z-directions, respectively
u', v'	turbulent fluctuating velocity in x and y-direction, respectively
u_*	friction velocity
U_i	velocity in x_i- direction
U_P	local purging flow rate
V	volume
$\dot{V}$	volume flow rate
v_i	covariant velocity component
v_i'	projected velocity component

x, y, z	Cartesian coordinates
x^+, y^+	non-dimensional distance from the wall (xu_*/ν, yu_*/ν)
x_i	Cartesian coordinate in the i-direction
x^i	general contravariant coordinate; there exist no equivalent covariant component
z_{front}	z-level which divides the lower and upper zone (see Section 3.4)

Greek symbols

β	coefficient of thermal expansion
Γ_ϕ	exchange coefficient of dependent variable
Δ_i	length of room in i-direction
$\delta_{1/2}$	y-value at which the velocity is $0.5U_{max}$
δ_i	half length of room in i-direction
ϵ	dissipation of turbulent kinetic energy
η	=y at the hot wall; =H-y at the cold wall
λ	slope
κ	von Karman's constant
μ, μ_t, μ_{eff}	dynamic viscosity (laminar, turbulent and effective, respectively)
ν	kinematic viscosity
ρ	density

σ_k, σ_T, σ_ϵ	turbulent Prandtl number for k, T and ϵ, respectively
τ	time
τ_{12}	turbulent shear stress in xy-plane
$\bar{\tau}$	average age in a system (room)
τ_n	nominal time constant of system (room) (=V/Q)
$\bar{\tau}_P$	local age at a point
τ_w	wall shear stress
υ	characteristic turbulent velocity
ϕ	dependent variable; cumulative distribution function for the age
φ	probability density function for the age
Ψ	$= k^{1/2}/L_t$, or stream function

Subscripts

E, P, W, WW, SW	referring to nodal locations
e, w	referring to locations on faces of control volumes
e	exit
eff	effective
in	inlet
max	maximum
w	wall

1. INTRODUCTION

Knowledge of the air movements in ventilated rooms is essential to be able to design a ventilation system. The object is to create an acceptable climate where suitable distribution of velocity, temperature, and concentration of contaminant prevail. The process of creating good indoor climate can, basically, be divided into two different categories: ventilation for a good air quality, and heating or cooling for thermal comfort. The air quality in ventilated rooms can be quantified by using ventilation parameters such as the local age and ventilation efficiency; calculation of ventilation parameters is carried out in this thesis.

There are two different types of ventilation system:

i) mixing flow systems, which give a nearly uniform air temperature and concentration of contaminants;

ii) displacement flow systems, which divide the flow in the room into two zones, a lower zone to which cool, clean air is continuously supplied, and an upper zone where contaminated, warm air recirculates.

One of the advantages of a displacement flow system is that it is efficient in supplying cooling (as the supply air is always cooler than that in the room), which is important since in most office buildings cooling is needed all year round (even in Scandinavia!). Numerical simulation of the flow in rooms with displacement flow systems is carried out in this thesis.

In order to be able to design a ventilation system which satisfies the requirement of good indoor climate, detailed knowledge of the flow pattern is of great help. In the past mostly experimental investigations were carried out, or simple calculation methods were used in which the velocity levels were estimated without actually solving the equations. In the 1970's researchers started to solve the flow equations using finite-difference methods [two-dimensional, isothermal calculations by e.g. Nielsen (1973), Holmberg et al. (1975); three-dimensional, isothermal calculations by e.g. Hjerthager (1979) and Gosman et al. (1980); two-dimensional, buoyant cal-

culations by e.g. Larsson (1977) and Nielsen et al. (1979); three-dimensional, buoyant calculations by e.g. Hjerthager (1979)]. In recent years calculation of the flow in ventilated rooms have become quite common.

There are special problems associated with predicting the flow in ventilated rooms. One problem is that the velocities, at least in some regions, are very small, which means it is possible that the flow is not fully turbulent. Consequently turbulence models which can account for viscous effects (so called "low Reynolds number turbulence models") should be used, not only near the walls, but also in the free (recirculating) flow regions. Turbulence models capable of taking account for viscous effects in free recirculating flows are, unfortunately, not available in the literature; an (preliminar) attempt to develop such a model is done in this thesis. In many cases, especially in displacement flow systems, it is important to accurately predict the heat transfer at the walls, a parameter which is essential for the performance of the ventilation system; this can probably only be done using low Reynolds number turbulence models. In this thesis low Reynolds number k-ϵ turbulence models are used when calculating the buoyancy driven flow in a rectangular cavity. Another problem when predicting the flow in ventilated rooms is that there is often a slow variation of the flow in time, which, when calculating the flow is often, if not always, not taken into account.

Rooms have mostly simple geometries which are readily described using Cartesian coordinates. However, this is not the case for larger halls such as concert halls, auditoriums, sport arenas (The Globe in Stockholm, for example). In order to be able to predict the flow in these type of halls, it is often necessary to use computer codes which allow description of the configuration in curvi-linear coordinates. Such a computer code is developed and applied to test problems in this thesis.

2. COMPUTATION METHOD

Finite volume methods are used in this thesis. The differential equations for fluid flow can all be cast in a general transport equation for the general variable ϕ (ϕ=velocity component, temperature, turbulence quantity, etc.) as

$$\frac{\partial}{\partial\tau}(\rho\phi) + \frac{\partial}{\partial x_i}\left(\rho U_i\phi - \Gamma_\phi \frac{\partial\phi}{\partial x_i}\right) = S^\phi \qquad (2.1a)$$

where τ, Γ_ϕ and S^ϕ denote time, exchange coefficient for ϕ, and source term for ϕ, respectively. All terms that are not of transient, convective or diffusive type - the pressure gradient in the momentum equations for example - are included in the source term. Equation (2.1a) is integrated over a control volume P, see Fig. 2.1. The control volume in Fig. 2.1 is, for convenience, taken to be rectangular, but can, in general, be of almost general form with four corners in two dimensions (see Fig. 1, Paper III). When, for example, the convective term $\partial(\rho U\phi)/\partial x$ is integrated over the control volume (unit length of the control volume in the y-direction), the following expression is obtained:

$$\int_w^e \frac{\partial(\rho U\phi)}{\partial x}dx = (\rho U\phi)_e - (\rho U\phi)_w$$

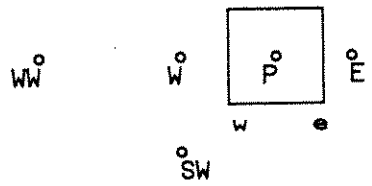

Figure 2.1. Control volume. The ϕ-variable is stored in the nodes (circles)

The problem now arises of how to estimate ϕ_w (ϕ is stored in the nodes W, P and E); the most natural choice is to use central differencing, i.e.

$$\phi_w = 0.5\ (\phi_P + \phi_W)$$

This choice leads to instability of the discretized equations when the local grid Reynolds number, $Re_{\delta x} = U_w\delta x/\nu$, exceeds two, which makes it almost

impossible to solve the equations numerically. However, there is a possibility as shown in Hedberg (1989). The value ϕ_w can be estimated in different ways, and the choice of method in estimating ϕ_w depends on which differencing method is used.

2.1 Different Differencing Schemes

Three different schemes used by the author (two in the thesis) are briefly presented below.

2.1.1 Hybrid Upwind/Central Differencing Scheme

This scheme approximates the convective terms using a central differencing scheme if the local grid Reynolds number is below two, and otherwise upwind differencing, i.e. (see Fig. 2.1)

$$\phi_w=\phi_W, \text{ if } |Re_{\delta x}|>2 \text{ and } U_w>0; \quad \phi_w=\phi_P \text{ if } |Re_{\delta x}|>2 \text{ and } U_w<0$$

$$\phi_w=\alpha\phi_P+ (1-\alpha)\phi_W, \text{ if } |Re_{\delta x}|<2$$

where α is an interpolation factor equal to 0.5 if the face w lies midway between W and P.

This scheme has been used in all papers in the thesis.

2.1.2 Quadratic Upstream-Weighted Interpolation

This scheme of Leonard (1979) utilizes a polynomial of the second order fitted to three nodes, two located upstream of the face, and one node located downstream; the scheme is thus a form of upwind scheme. It combines the accuracy of central differencing (second order accuracy) with the inherent stability of upwind differencing (due to its upwind character). For a uniform grid the ϕ_w is approximated as:

$$\phi_w= -0.125\phi_{WW}+ 0.75\phi_W+ 0.375\phi_P, \quad U_w>0$$

$$\phi_w= 0.375\phi_W+ 0.75\phi_P- 0.125\phi_E, \quad U_w<0$$

This scheme has been used in the thesis in Paper VI in the momentum and temperature equations. The resulting form of the coefficients for a non-uniform grid is given in Appendix in Paper VI.

2.1.3 Skew-Upwind Difference Scheme

This is only a first-order scheme of Raithby (1976), but it has the advantage of reducing one of the most important and frequent agencies of numerical diffusion for two-dimensional recirculating flows: flow-to-grid skewness. The basic idea of the scheme is to apply upwind differences in a vectorial rather that in a componential sense. If, for example, the angle between the velocity vector at face w and the x-axis (see Fig. 2.1) is 45^o (i.e. $U_w=V_w>0$) ϕ_w is approximated as:

$$\phi_w = 0.5(\phi_W + \phi_{SW})$$

This scheme has been used by the author elsewhere (Davidson, 1988) in the momentum equations.

2.2 Solving the Discretized Equations

When all terms in Eq. (2.1a) were integrated over the control volume P in Fig. 2.1, the partial differential equations were cast, using various approximations, into algebraic equations for discrete points (control volumes); the equations were discretized. They have the form

$$a_P\phi_P = \sum a_{nb}\phi_{nb} + S_C^\phi \qquad (2.1b)$$

where a_{nb} (nb=neighbour) contain convective and diffusive contributions, and S_C^ϕ is the constant part of the source term. The a_P-coefficient has the form

$$a_P = \sum a_{nb} - S_P^\phi$$

where S_P^ϕ is the proportional part of the source term, so that the total source can be written

$$S^\phi = S_P^\phi \phi + S_C^\phi$$

One discretized equation [Eq. (2.1b)] is derived for each variable ϕ.

The coupling between pressure and velocity is handled using the SIMPLE procedure (or either of its derivatives, SIMPLER and SIMPLEC). The main features of the solution method can be summarized as:

i) use of staggered grids for the velocities in order to avoid unphysical oscillations in the pressure field;

ii) formulation of the difference equations in implicit, conservative form;

iii) rewriting of the continuity equation into an equation for pressure correction, where the latter is used to correct the pressure and the velocities; and

iv) iterative solution of the equations using the Tri-Diagonal-Matrix Algorithm line-by-line solver.

2.3 The k-ε Turbulence Model

In most of the thesis the standard k-ε turbulence model is used; in Paper II a new one-equation turbulence model is developed, and in Paper VI two different low Reynolds number k-ε models are used.

The time averaged momentum equations can be written

$$\frac{\partial}{\partial \tau}(\rho U_i) + \frac{\partial}{\partial x_j}(\rho U_i \phi) = -\frac{\partial p}{\partial x_i} + \frac{\partial}{\partial x_j}\left(\mu \frac{\partial U_i}{\partial x_j} - \rho \overline{u_i' u_j'}\right)$$

which contain the unknown Reynolds stress tensor, $\rho \overline{u_i' u_j'}$, which must be modelled, in order to close the equation system. In eddy viscosity turbulence models (such as the k-ε model) the Reynolds stress tensor is expressed using the Boussinesque eddy viscosity concept

$$\rho \overline{u_i' u_j'} = -\mu_t\left(\frac{\partial U_i}{\partial x_j} + \frac{\partial U_j}{\partial x_i}\right) + \frac{2}{3}\delta_{ij}\rho k$$

where δ_{ij} is Kronecker's delta. The eddy (turbulent) viscosity, μ_t, is, using dimensional analysis, obtained as

$$\mu_t = \rho \upsilon \ell$$

where υ and ℓ denote a turbulent characteristic velocity and length scale, respectively. The turbulent velocity is taken as the square-root of the the

turbulent kinetic energy, $\sqrt{k}$, and the turbulent length scale can, by using dimensional analysis, be taken as

$$\ell \sim k^{3/2}/\epsilon$$

where ϵ denotes the dissipation of turbulent kinetic energy. Now an expression for turbulent viscosity can be written as

$$\mu_t = c_\mu \rho \, k^2/\epsilon \tag{2.2}$$

where c_μ is a constant. Two partial differential equations for the two new unknown, k and ϵ, can be derived; unknown terms are modelled, and the resulting modelled k and ϵ-equations can be written (see, e.g., Rodi, 1980)

$$\frac{\partial}{\partial \tau}(\rho k) + \frac{\partial}{\partial x_i}(\rho U_i k) = \frac{\partial}{\partial x_i}\left[\left(\mu + \frac{\mu_t}{\sigma_k}\right)\frac{\partial k}{\partial x_i}\right] + P_k - \rho\epsilon \tag{2.3a}$$

$$\frac{\partial}{\partial \tau}(\rho \epsilon) + \frac{\partial}{\partial x_i}(\rho U_i \epsilon) = \frac{\partial}{\partial x_i}\left[\left(\mu + \frac{\mu_t}{\sigma_\epsilon}\right)\frac{\partial \epsilon}{\partial x_i}\right] + \frac{\epsilon}{k}\left(c_{\epsilon 1} P_k - c_{\epsilon 2} \rho\epsilon\right) \tag{2.3b}$$

where the production term, P_k, and the constants have the form

$$P_k = \mu_t\left(\frac{\partial U_i}{\partial x_j} + \frac{\partial U_j}{\partial x_i}\right)\frac{\partial U_i}{\partial x_j}$$

$$\sigma_k = 1.0, \; \sigma_\epsilon = 1.3, \; c_\mu = 0.09, \; c_{\epsilon 1} = 1.44, \; c_{\epsilon 2} = 1.92$$

In buoyancy affected flows additional terms appear in the k and ϵ-equations.

2.4 The Wall Functions

The k-ϵ model presented in Section 2.3 is applicable only in regions with high turbulent Reynolds number, μ_t/μ. Close to the walls where viscous effects become dominant this model cannot be used. Therefore wall functions are used at walls. Another reason for using wall functions, and perhaps more important, is that it is computationally much cheaper to use wall functions rather than resolving the flow in the boundary layer by locating many grid lines in this region. When using wall functions it is usually

sufficient to cover the boundary layer with 2 to 5 grid lines (in the normal direction), whereas when the flow in the boundary layer is to be resolved 15 to 30 grid lines must be used. When the flow in the boundary layer is resolved an extended turbulence model - a low Reynolds number (see Paper VI) - must be used.

The wall functions in this thesis are of standard type (see e.g. Rodi, 1980), where the production of turbulent kinetic energy, P_k, and the dissipation term, ϵ, in the k-equation [see Eq. (2.3)] are assumed to balance each other so that

$$P_k = \rho\epsilon \tag{2.4}$$

The production term is written as

$$P_k = \mu_t \left(\frac{\partial U}{\partial y}\right)^2 \tag{2.5}$$

which, together with the assumption of constant shear stress in the boundary layer

$$\tau_w = \rho u_*^2 = \mu_t \frac{\partial U}{\partial y} \tag{2.6}$$

gives

$$P_k = [\rho u_*^2]^2/\mu_t \tag{2.7}$$

Equation (2.7) into Eq. (2.4) using the relation for μ_t in Eq. (2.2) gives

$$k = c_\mu^{-1/2} u_*^2$$

The expression for ϵ is obtained from Eqs. (2.4-6) as

$$\epsilon = u_*^2 \frac{\partial U}{\partial y}$$

Using the law of the wall gives the velocity gradient

$$\frac{\partial U}{\partial y} = \frac{u_*}{\kappa y}$$

where κ is von Karman's constant, so that, finally

$$\epsilon = \frac{u_*^3}{\kappa y}$$

For the velocity components parallel to the wall, the wall shear stress, $\tau_w = \rho u_*^2$ is used as boundary condition; the friction velocity, u_*, is obtained from the law of the wall.

The wall function used can be summarized as:

i) the grid line near the wall for which the wall function is used should be in the region $30<y^+<400$.

ii) u_* is obtained, in an iterativ manner, from the law of the wall

$$\frac{U}{u_*} = \frac{1}{\kappa} \ln (9.0 \frac{u_* y}{\nu})$$

iii) the turbulent kinetic energy is set as

$$k = c_\mu^{-1/2} u_*^2$$

iv) the dissipation is set as

$$\epsilon = \frac{u_*^3}{\kappa y}$$

v) the shear stress

$$\tau_w = \rho u_*^2$$

times surface area is included as a sink in the equation for the velocity component parallel to the wall.

3. SUMMARY OF PAPERS

3.1 Paper I

In this paper numerical simulation of two new ventilation parameters - the local purging flow rate and the local age - is carried out. The two ventilation parameters were introduced by Sandberg and Sjöberg (1983) and Sandberg (1981). The local purging flow rate, U_p, is the local net flow rate at which air is supplied, from the inlet, to an arbitrary control volume in the room. The local age at an arbitrary point is the time τ that has elapsed since the air passing this point entered the room. There is, at the present time, no practical method for measuring the local purging flow rate. The local mean age distribution is, however, relatively easy to obtain experimentally, and has been investigated by Sandberg (1984), whose results show that knowledge of the distribution of the local age provides useful information on how air and contaminants spread in ventilated rooms. Such a concept of age is therefore a valuable tool in evaluating the performance of different ventilation schemes.

The distribution of the local age has been calculated in two three-dimensional, buoyantly ventilated rooms in which Sandberg (1984) has measured the temperature and the local mean age. In one of the cases (see Fig. 3.1a) the inlet and the outlet are situated near the ceiling (hereafter denoted by Case HI; High Inlet). The incoming air was warmer than that of the room and the windows were cold, simulating a ventilation situation in winter. This configuration was expected to give very poor ventilation with high average age for the room. In the other case (see Fig. 3.1a) the inlet was placed near the floor (hereafter denoted by LI; Low Inlet) and the outlet was situated near the ceiling as in Case HI. The incoming air was colder than the air in the room and the windows were warm, simulating a ventilation situation in summer. This configuration was expected to give low average local age for the room.

As there is not yet an experimental method for measuring the local purging flow rate, it was expected that a numerical simulation of the field of local purging flow rate might enhance the understanding of the concept and give an idea of its future use and application. It is very expensive to calculate the local purging flow rate since a separate calculation has to

be made for each cell involved. For this reason, the local purging rate field was calculated in a two-dimensional iso-thermally ventilated room (hereafter denoted Case 2D, see Fig. 3.1b).

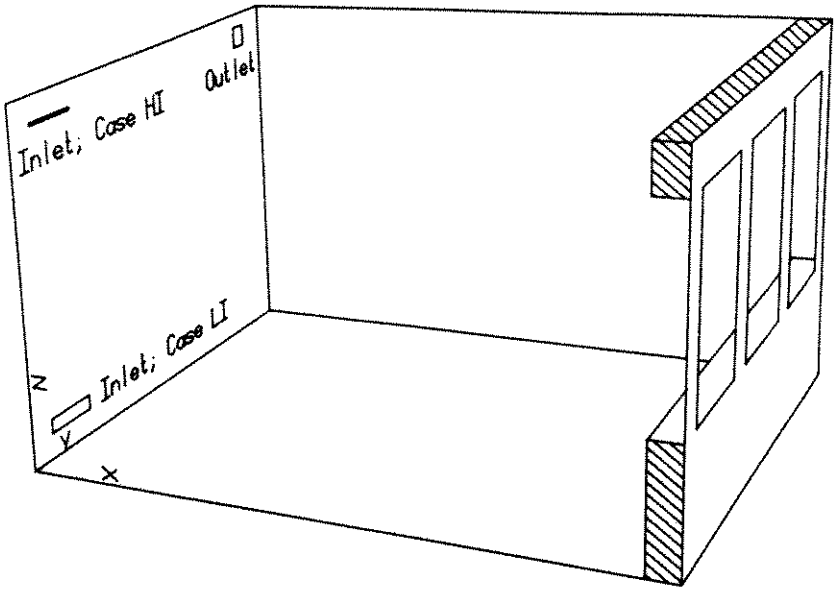

a)

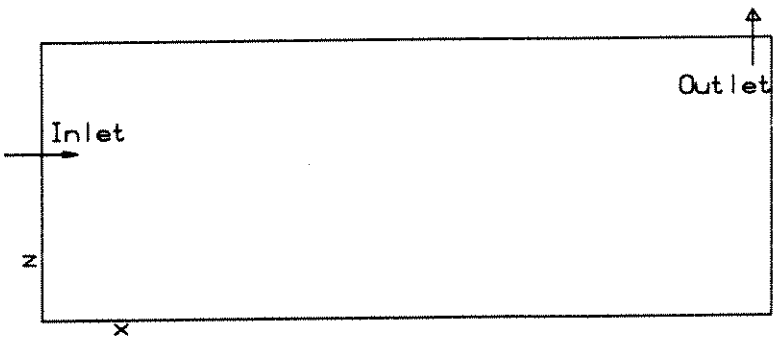

b)

Figure 3.1. Flow configurations. a) Cases HI and LI. b) Case 2D.

The expression for the local age, $\bar{\tau}_p$, for the step-up method can be derived (see Section 3 in Paper I) as

$$\bar{\tau}_p = \int_0^\infty (1-c_p(\tau)/c_0)d\tau$$

where c_p and c_0 denote the concentration at an arbitrary point (or control volume), and the concentration in the supply air, respectively.

The concept of the local purging flow rate, U_p, can be understood as the net rate at which a dynamically passive contaminant is 'flushed' out of the system from P, or equivalently, the rate at which fresh air is supplied to P, where P is an arbitrary control volume within the system. The local purging flow rate is obtained by introducing a source of a dynamically passive contaminant at P where U_p is to be obtained. An expression for U_p is easily obtained by setting up a mass balance for the contaminant. If a source $\dot{m}_p$ of contaminant is placed at control volume P, then $\dot{m}_p$ must also, as demanded by continuity when steady state has been reached, exit the system, which gives $\dot{m}_p = Qc_e$ (Q denotes the total ventilation mass flow rate, which is equal to the mass flow rate through the inlet; c_e denotes the concentration at the exit). $\dot{m}_p$ is obtained from the definition of U_p as $\dot{m}_p = U_p c_p$, so that

$$U_p = \dot{m}_p/c_p = Q\,\frac{c_e}{c_p}$$

Both the age and the local purging flow rate fields are simulated using dynamically passive contaminants, which means that the flow field is not affected by the contaminants. This makes it possible to calculate the flow field first and then use the calculated flow field whene calculating $\bar{\tau}_p$ and U_p.

Since the calculated U_p is dependent on the size and form of the control volume P where $\dot{m}_p$ is introduced (see Appendix in Paper I) a uniform grid should be used, i.e. all control volume sides should be of equal length. In the present work the flow field was calculated using unequally spaced grid lines. When the U_p-field was calculated, a grid with all control volume sides equal was used. The velocity field for this 'U_p- grid' was obtained by interpolation from the 'velocity grid' so as to satisfy continuity.

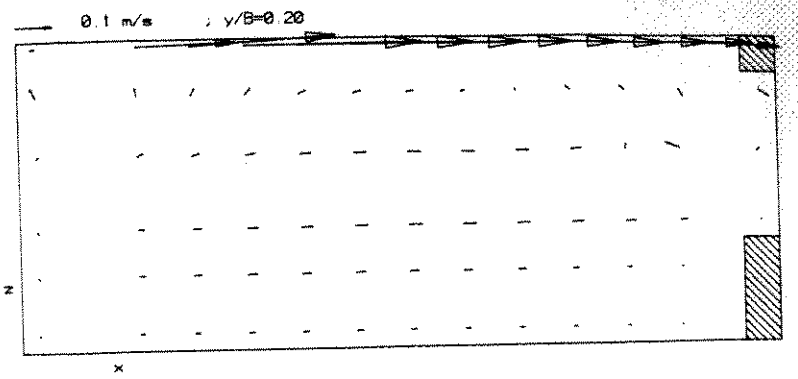

a)

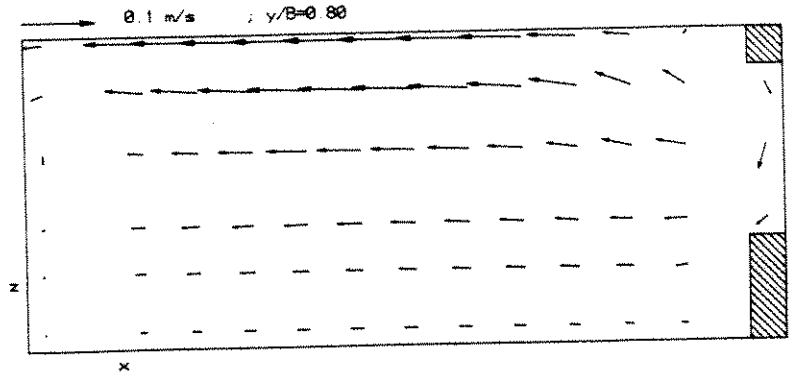

b)

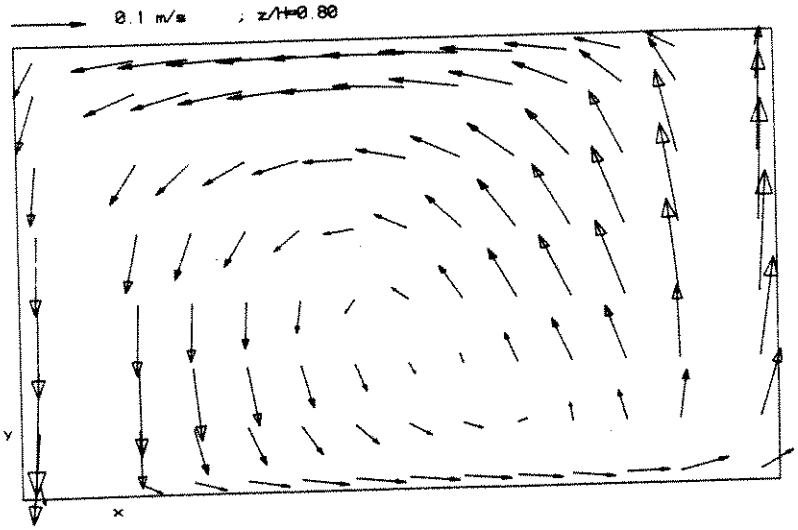

c)

Figure 3.2. Calculated velocity vectors. Case HI.

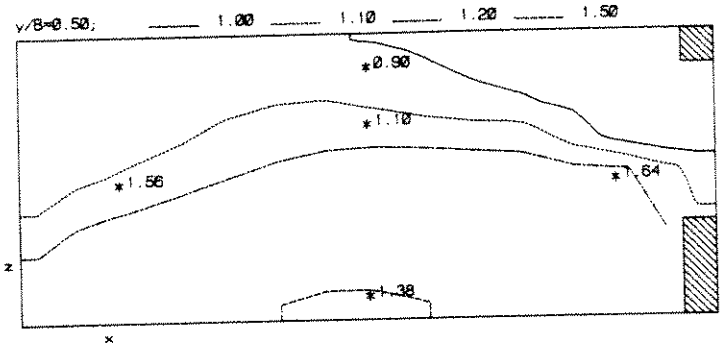

Figure 3.3. Predicted contours of local age scaled with τ_n. Case HI. Expts. by Sandberg (1984) at stations marked with stars.

In Fig. 3.2 (see also Figs. 2 and 3 in Paper I) velocity vectors for Case HI are drawn. From these plots it can be seen that the wall jet following the ceiling hits the wall opposite the inlet and that the flow is forced along this wall. The flow does not fall down towards the floor because of the upwards directed buoyancy force. It reaches the side wall at y=B and turns left towards the outlet. This large counter-clockwise vortex near the ceiling is spread by friction in the whole room; the result is a counter-clockwise vortex at each z-level, with little fluid interchanged between the different z-levels.

This flow pattern results in high local age near the floor and gradually lower $\bar{\tau}_p$ near the ceiling as can be seen in Fig. 3.3. The agreement between predictions and experimental data is not very good, with local discrepancies up to 25%. While numerical predictions show an almost monotonic increase in age of the air with decreasing z, the experiments show maximum age in the middle (in the z-direction, that is) of the room. This may indicate that the predicted flow pattern is more stratified than that in the experiments. The predicted average age for the room $\bar{\tau}/\tau_n$=1.14 (τ_n denotes the nominal time constant, which is equal to the local age at the exit), is in fairly good agreement with the experimental value 1.3.

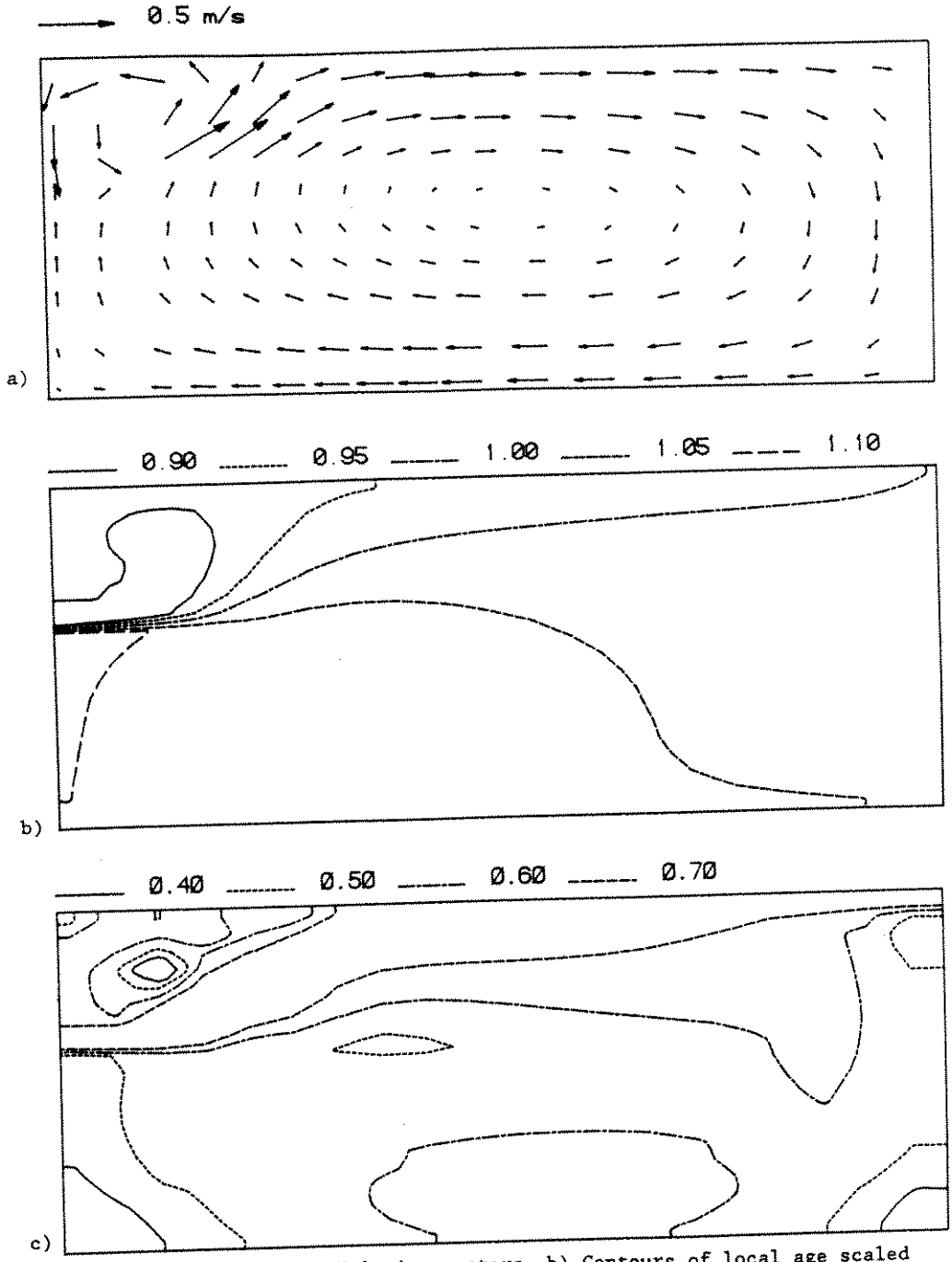

Figure 3.4. Case 2D. a) Velocity vectors. b) Contours of local age scaled with τ_n. c) Contours of local purging flow rate scaled with Q.

The discrepancies between predicted and experimental local age in Case LI are of the same order as in Case HI. The reason for these discrepancies is probably to be found in the discrepancies between the predicted and experimental velocity fields, which are probably due to a combination of inaccuracies in the predictions (such as the turbulence model, the wall-functions) and the experiments (uncertainty in the inlet conditions, incomplete homogenous mixing of the contaminant in the initial transient, etc.; see Paper I). Fontaine et al. (1988) have recently carried out an experimental and numerical study of the local age in a two-dimensional isothermally ventilated room. They obtain good agreement between predictions and experiments in the larger part of the room; in the wall jet region, however, there are discrepancies of up to 30 percent. Fontaine et al. believes this is due to instabilities observed in the experiments owing to the low Reynolds number. This can also be the case in the experiments by Sandberg (1984).

The predicted velocity vectors, the predicted local age-field, and the predicted U_p-field for Case 2D are shown in Fig. 3.4. Comparing the local age field and the local purging flow rate field, it can be concluded that the main features of the ventilation situation are shown by either of the two fields; they both indicate that the flow in the lower half of the room is more stagnant than in the upper half. The largest differences between the two fields occur in the regions near the upper two corners. In the region of the upper left corner the gradient of U_p is large: to the left of the point where the jet reattaches to the ceiling (where the flow when reaching the ceiling turns back towards the inlet wall, see Fig. 3.4a) low values prevail, while to the right of this point (where the flow goes more directly towards the outlet) U_p has higher values; the age of the air is low since it does not take long time for the air to reach the region near this corner. Below the outlet, where the flow is directed from the outlet, U_p attains low values whereas the air is here not very 'old'.

Sandberg and Sjöberg (1983) have proved, theoretically, that in regions where $\bar{\tau}_p/\tau_n > 1$ the product of U_p and $\bar{\tau}_p$ should be less than or equal to the volume of the room, i.e.

$$U_p \bar{\tau}_p \leq V, \text{ or, } U_p/Q\ \bar{\tau}_p/\tau_n \leq 1; \quad \text{when } \bar{\tau}_p/\tau_n > 1 \qquad (3.1)$$

where V denotes the volume of the room. This relation restricts U_p more severely for higher values of $\bar{\tau}_p$. The relation in Eq. (3.1) was confirmed, but as the calculated $\bar{\tau}_p$ nowhere in the room is especially large ($\bar{\tau}_p \leq 1.1\tau_n$ everywhere) this confirmation is of little value. In order to 'prove' or 'disprove' the relation in Eq. (3.1) the local age field and the U_p-field should be calculated in ventilated rooms where regions of much higher values of $\bar{\tau}_p$ occur.

The local age and the local purging flow rate have been calculated in a later work (Davidson and Olsson, 1987) in cases where the local age was very high, and the relation was also confirmed for these cases.

3.2 Paper II

In this paper a new one-equation turbulence model is developed and tested. The turbulent viscosity, μ_t, is obtained as

$$\mu_t = c'_\mu \rho \sqrt{k}\, L_t$$

where c'_μ is a constant and k and L_t denote the turbulent kinetic energy, and turbulent length scale, respectively. The turbulent kinetic energy is obtained from the standard k-equation, and a new equation is developed for L_t. This equation is based on an analogy of von Karman's formula

$$L_t = -\kappa \frac{\partial U/\partial y}{\partial^2 U/\partial y^2} \qquad (3.2a)$$

where y is the coordinate normal to the wall, U the mean velocity parallel to the wall, and κ the von Karman constant. A variable Ψ with the same dimension as the velocity gradient $\partial U/\partial y$ is formed as

$$\Psi = k^{1/2}/L_t$$

which, in analogy with Eq. (3.2a), yields

$$L_t = -\kappa \frac{\Psi}{\partial \Psi/\partial y} \qquad (3.2b)$$

This equation has been used by Bobyleva et al. (1965) when calculating atmospheric boundary layers; no comparison with experiment has, however, been carried out. Equation (3.2b) can be rewritten as

$$\Psi^{-2}\frac{\partial \Psi}{\partial y} = -\kappa k^{-1/2}$$

which can be integrated so that

$$L_t = \kappa k^{1/2}\int k^{-1/2} dy + f(x) \qquad (3.3)$$

where f(x) is an integration function. Since L_t is a turbulent length scale, the integral in Eq. (3.3) cannot be taken from the wall through the viscous sublayer. The lower limit of the integral is taken to be in the inertial sublayer, approximately $30 < y^+ < 100$, where $L_t = \kappa y$ is the appropriate boundary condition for all x, so that

$$L_t = \kappa k^{1/2}(y)\int_{y_p}^{y} k^{-1/2}(y')dy' + \kappa y_p \qquad (3.4)$$

It may be noted that Eq. (3.4) is easily extended so as to be valid in the viscous sublayer as well; this is done by replacing κy_p with the well-known van Driest's formula $\kappa y_p[1-\exp(-y^+/26)]$.

It was found that the length scale equation in Eq. (3.4) is not appropriate for parabolic near wall flows. Three modifications of Eq. (3.4) were tested in Davidson (1986) and one of these is used in Paper II; this modified length scale equation has the form

$$L_t = \min\left(\kappa k^{1/2}(y)\int_{y_p}^{y} k^{-1/2}(y')dy' + \kappa y_p,\ 0.09\delta\right) \qquad (3.5)$$

where δ is the width of the layer in the case of the flat-plate boundary layer and the plane wall jet; in the case of the plane channel it denotes the half-width of the channel.

In calculations of elliptical flows (two- or three-dimensional) there are two or three coordinate directions which may be relevant when calculating L_t in Eq. (3.5). $L_{t,i}$ is formulated so that

$$L_{t,i} = \min\left(\kappa\, k^{1/2}\int_{n_{i,p}}^{n_i} k^{-1/2} dn_i + \kappa n_{i,p}, 0.09\Delta_i\right)$$

where n_i is the normal co-ordinate from wall 'i', Δ_i the length of the room in n_i-direction, and subscript p denotes a point within the inertial sub-layer. Four (two-dimensional calculations) or six (three-dimensional calculations) different $L_{t,i}$ can be calculated and L_t is taken as the minimum of these, i.e.

$$L_t = \min(L_{t,i}), \quad i = -1, 1, -2, 2 \ (,-3, 3)$$

It actually suffices to calculate $L_{t,i}$ for the two (three) nearest walls.

The model is tested in three parabolic flows: the flat-plate boundary layer, the plane wall jet, and the fully developed flow in a plane channel. The model is also tested in four elliptical flows: three two-dimensional rooms, and one three-dimensional. The model is shown to give as good agreement with experiments - better in case of the wall jet - as the k-ϵ model for the parabolic flows, and to predict the elliptical flows sufficiently well for engineering purposes. In the elliptical calculations the CPU time using the k-ϵ model was found to be up to more than twice as much compared with when the one-equation model was used.

The predicted mean velocity profiles and turbulent shear stress (for the wall jet) are compared with experimental data in Fig. 3.5. It can be seen that the predictions with the one-equation model are slightly superior to those obtained with the k-ϵ model. The spreading rate of the wall jet is also better predicted with the one-equation model than with the k-ϵ model; $d\delta_{1/2}/dx$ ($\delta_{1/2}$ denotes the y-value where the velocity is half of the maximum velocity across the layer) was 0.094 and 0.084 for the k-ϵ model and the one-equation model, respectively. These values should be compared with the experimental values $d\delta_{1/2}/dx$=0.071-0.075 (Launder and Rodi, 1981).

In Fig. 3.6 the predicted velocity profiles are compared with experiments for a two-dimensional buoyantly ventilated room. The inlet is located at the top of the left wall, and the outlet is located at the bottom of the right wall. The two turbulence models perform, as can be seen, equally well.

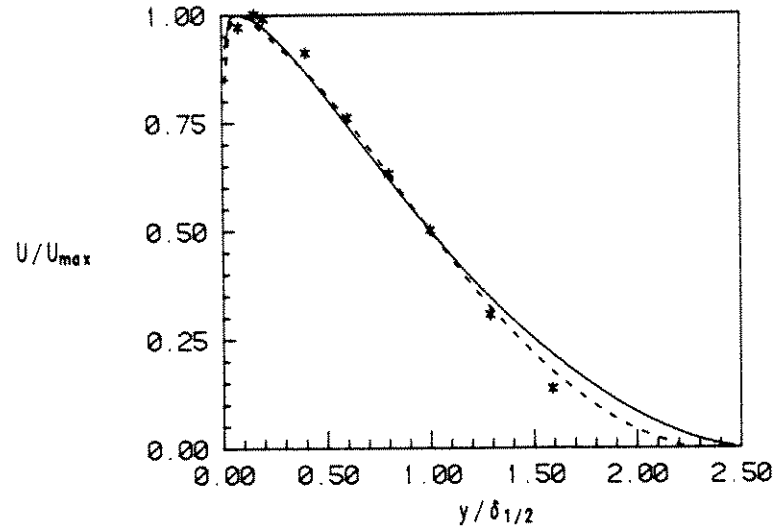

a)

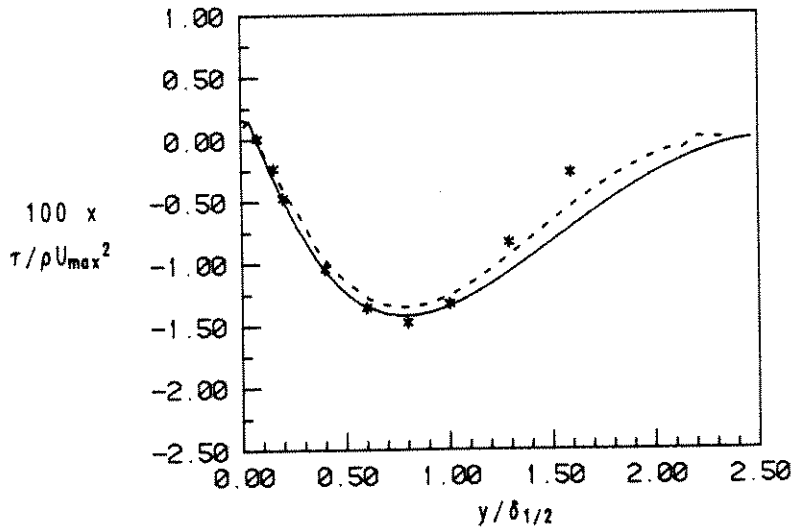

b)

Figure 3.5. Wall jet. —— k-ε. - - - One-equation model. * Experiments by Tailland and Mathieu (1967). a) Velocity profile. b) Turbulent shear stress.

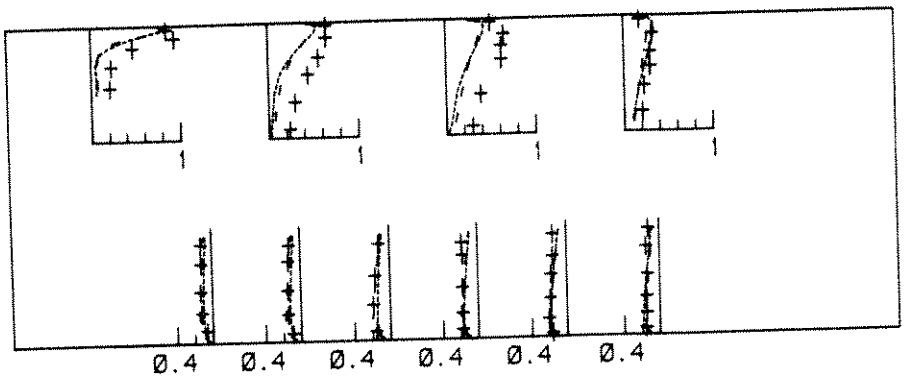

Figure 3.6. Profiles of absolute velocity scaled with U_{in}. — — — k-ε. ..... One-equation model. + Experiments by Hanel (1980).

3.3 Papers III and IV

In these papers a novel finite-volume formulation of the Navier-Stokes equations for general non-orthogonal curvilinear coordinates is derived, and applied to test problems. Much work has been done in developing and applying finite-volume methods to complex geometries. In some of the work, general orthogonal coordinates have been used. The advantage of using orthogonal coordinates rather than non-orthogonal coordinates is that the equations become much simpler; the disadvantage is reduced flexibility when generating the grid.

Other researchers have used non-orthogonal coordinate systems. A choice has to be made when representing the velocity vector, and some have chosen covariant velocity components, others contravariant and still others physical velocity components. Using covariant velocity components means that the pressure-velocity coupling becomes relatively easy to handle at the expense of the more complicated expression of convective and diffusive fluxes. For contravariant and physical velocity components, the problems are reversed. Covariant velocity components have been chosen in this work.

The approach taken here is to set up a local rectilinear coordinate system, where the coordinate axis, in the direction of the $(v_l)_e$-velocity component, is kept constant in the neighbourhood of point e. This means that

most of the terms due to the curvature/divergence and non-orthogonality of the grid vanish. The procedure of keeping the coordinate axis constant (i.e. $\vec{g}_i$ = constant) in the immediate vicinity of point e affects the convected velocity only. The convecting velocity (convection, i.e. dot product of the velocity vector and the area vector) is calculated without any change of the base vectors. This is also the case for the diffusion term.

This approach has previously been adopted by Karki (1986) (see also Karki and Patankar, 1988a,b) and partly by Malin et al. (1985) (see also Hedberg et al., 1988). In neither of these works was the mathematical derivation shown.

The momentum equations for turbulent flow in general coordinates, using covariant components can be written (Aris, 1962)

$$(\rho g^{jk} v_i v_j)_{,k} = -\frac{\partial p}{\partial x^i} + (\mu_{eff}\, g^{jk} v_{i,j})_{,k} \qquad (3.6)$$

where g^{jk} denotes the contravariant components of the metric tensor. Here the subscripts (i,j,k) denote covariant components, and superscripts (i,j,k) denote contravariant components; this convention is used throughout this section. The comma notation is used for denoting the covariant derivative. In Paper III it is shown that if a local coordinate system is used so that the direction of the neighbouring velocities, v_{inb} (i = co-ordinate direction, nb = neighbour), are kept the same as that of the velocity (v_{1e} or v_{2n}) being solved (see Fig. 3.7), Eq. (3.6) can be integrated and rewritten so that

$$\int_A g^{jk}\left(\rho v_i v_j - \mu_{eff}\frac{\partial v_i}{\partial x^j}\right) n_k dA + \int_A p\, n_i dA = 0$$

where A denotes the bounding area of the control volume with the volume V, and $\vec{n}$ is its normal vector.

The neighbouring velocities with a prime (see Fig. 3.7) denote velocity vectors projected on $\overrightarrow{PE}$. The velocity v'_{lee}, for instance, is calculated as

$$v'_{lee} = \vec{v}\cdot\overrightarrow{PE}$$

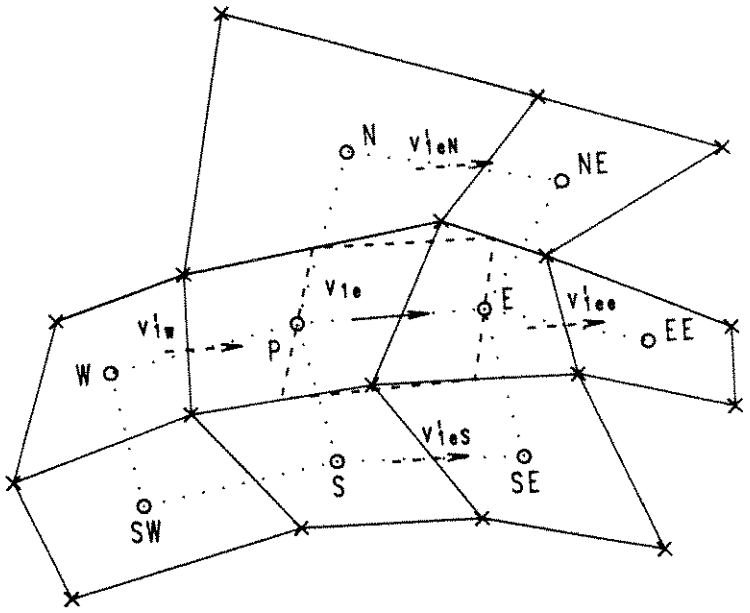

Figure 3.7. The grid. The dashed arrows show the neighbouring velocity vectors projected on $\overrightarrow{PE}$, i.e. v'_{lee}, v'_{lw}, v'_{leN} and v'_{leS}. The crosses define the corners of the scalar control volumes, and the circles define the scalar nodes. The position of a scalar node is defined as the average of its four cell corners. The dotted lines which connect these nodes define the direction of the covariant base vectors, $\vec{g}_i$. The v_1-control volume is staggered in the positive x^1-direction; it is outlined with dashed lines. Its east face, for example, is defined as being midway between the east faces of scalar control volumes P and E.

where $\overrightarrow{PE}$ ($=\vec{g}_{1e}$) is a covariant unit vector. More details on the code can be found in Davidson and Hedberg (1988).

In most studies on deriving discretised equations for flow in complex geometries, the terms due to curvature, divergence and non-orthogonality of the grid have been included using Christoffel symbols and metric tensors. Since the number of these terms is rather large, this is a very cumbersome procedure and may also be inaccurate (there appear terms containing up to

the third derivative of the grid coordinates). This is not the case with the present formulation.

It is well known that upwind differencing gives rise to numerical diffusion. For polar coordinates, or curved grids in general, another type of error occurs and becomes especially serious when the flow is not aligned with the grid lines. Even if the magnitude of the velocity component is well-approximated by estimating the face value of v_l with its node value, the direction of v_l is not. This was recognised by Galphin et al. (1986), who suggested the introduction of a correction velocity, weighted with a factor ω ($0<\omega<1$) depending on the curvature of the flow relative to the grid (cylindrical polar grid). The value of ω is zero if the flow is aligned with the grid.

In the present work this problem is solved in a more general and straightforward way. The velocity vectors, $\vec{v}_{nb}$ (nb=neighbour), are projected in the direction of the velocity component at the control volume e. This means that all the neighbours, v'_{lnb}, of v_{le}, have the same direction. In this way a solution is found to the problem of estimating a face value of v_l with an incorrect direction.

It is shown that, when using upwind differencing, the use of projected velocities gives better results than when curvature effects are included in the source term, which is demonstrated in Section 3.3.1.

3.3.1 Uniform Flow Using a Cylindrical Grid

The configuration with the grid is shown in Fig. 3.8. The viscosity is set to zero since in this case the errors for upwind differencing are to be estimated. The density is constant and the boundary conditions are:

$$v_2 = v_r = U\cos\alpha,\quad v_1 = v_\varphi = -U\sin\alpha$$

which is also, together with p=0, the exact solution.

The flow has been calculated with the standard treatment of curvature terms, and with the procedure of projecting the velocities. The maximum error in the calculated velocities is 8.5% and 0.5% of U for the two cases respectively. In Fig. 3.9 the contours of the pressure are presented, which

shows that the formulation in the present study is superior to conventional treatment of curvature effects.

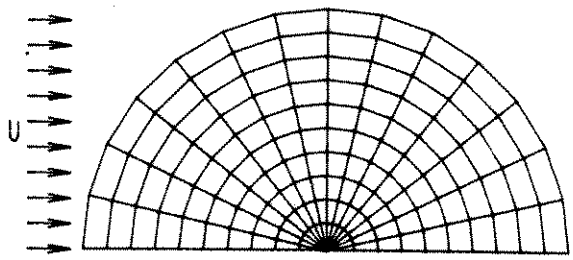

Figure 3.8. Configuration with grid (uniform flow).

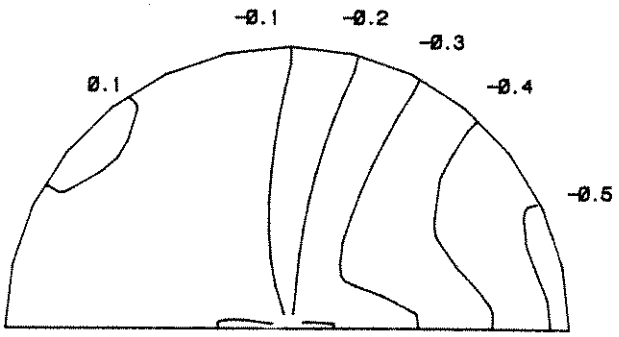

a)

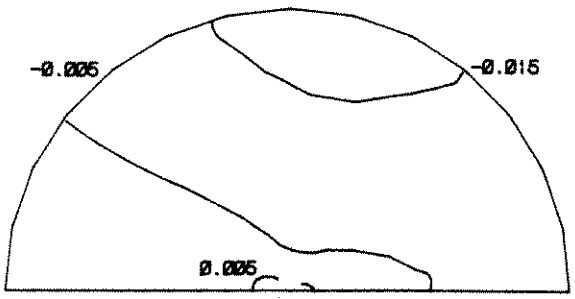

b)

Figure 3.9. Contours of isobars. Numbers denote pressure scaled with dynamic pressure, $\rho U^2/2$. a) non-projected velocities b) projected velocities

3.3.2 A Non-Rectangular Two-Dimensional Room

The configuration with the grid is shown in Fig. 3.10, and in Fig. 3.11 the calculated and the experimental velocity profiles are shown. The agreement between predictions and experiments is, as can be seen, good.

The local age for this case has also been calculated in Davidson (1989).

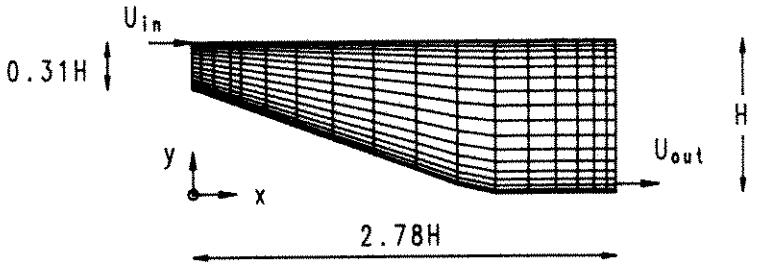

Figure 3.10. Configuration with grid (non-rectangular room)

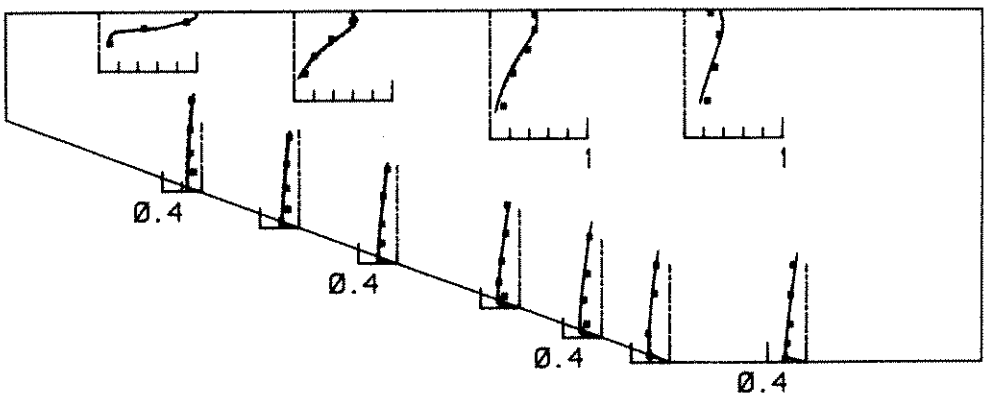

Figure 3.11. Velocity profiles of the absolute velocity, $|\vec{v}|/U_{in}$. Solid lines: 33 x 33 node grid; dotted lines: 53 x 62 node grid; markers: experiments by Hanel and Köthnig (1983).

3.4 Paper V

In this paper the flow in a new type of ventilation system - displacement flow system - is numerically simulated. Since in Scandinavia displacement flow systems are now increasingly replacing the traditional mixing flow systems, it is of great interest to perform a numerical study of the flow in a displacement system. The two ventilation systems are briefly described below.

Mixing flow system

In these systems the air is supplied through a small inlet device near the ceiling (or in the ceiling) at relatively high velocity. A jet, or wall jet, is formed and it entrains the air in the whole room. This gives a nearly uniform distribution of temperature and contaminant throughout the room.

Displacement flow systems

The air is supplied at low velocity through a large inlet device near the floor; the temperature of the supply air is cooler than that in the room. The cool air is heated by the heat source (persons, machinery, lighting etc.). A plume is formed above the heat source (see Fig. 3.12): owing to the higher temperature there (the density is lower) than in its surroundings. The volume flow rate in the plume entrains the surrounding air, and the flow rate in the plume increases with height. At the vertical level z_{front} (the z-level of the front, see Fig. 3.12) the flow rate in the plume is equal to total ventilation flow rate. The flow in the room is divided into two zones at the front: a lower zone with clean cool supply air, and an upper zone where contaminated heated air is recirculating.

The object of the present study is to calculate the flow in such a configuration using a finite volume method, and to compare the calculated results with experimental data (Sandberg, 1988) in order to investigate how well such flows can be predicted using finite-difference methods. No such investigation has, to the best of the author's knowledge, previously been carried out.

The experiments (and the calculations) were carried out in a water box model; water was chosen as medium because it is easier to carry out visualization experiments in water.

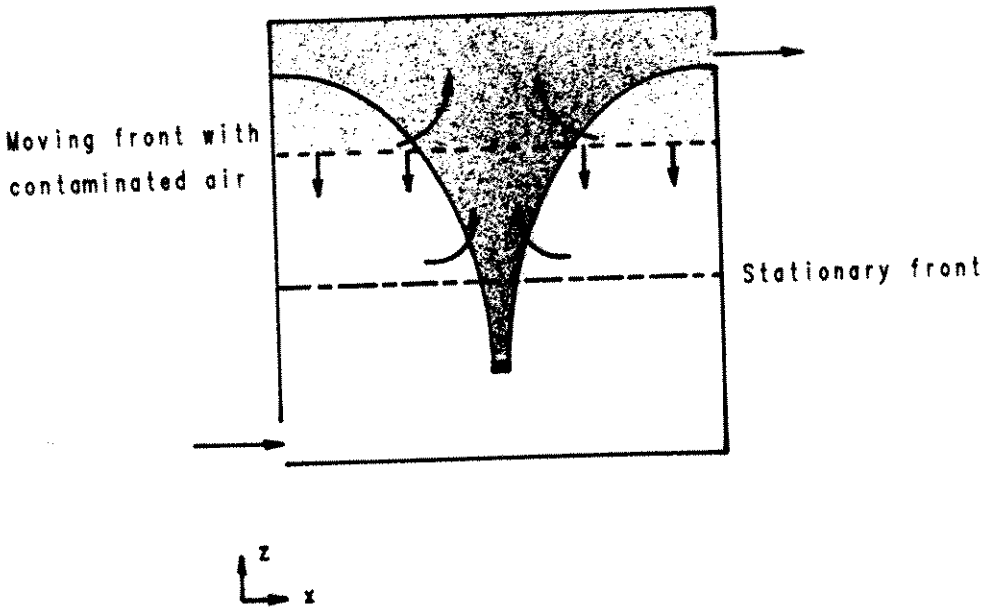

Figure 3.12. A schematic figure for a displacement flow system.

The flow in a three-dimensional room is calculated, see Fig. 3.13. The widths of both the inlet and the outlet are equal to the width of the room. In the middle of the room near the floor a heat source is introduced (dotted region in Fig. 3.13). The medium is water, and the inlet temperature is around 13°C. Sandberg and Lindström (1987) and Sandberg (1988) have carried out a number of experimental investigations on this configuration in which vertical temperature profiles have been measured; the calculated results are compared with these data.

The results for one case (Case Q200, see Paper V) are briefly presented below. The calculated velocity vectors are shown in Fig. 3.14. It can be seen that the flow goes from the inlet towards the opposite wall. Near the heat source ($x/L \approx 0.5$, $y/L \approx 0.5$), the flow is, due to buoyancy, lifted up towards the ceiling, and a turbulent buoyant plume is formed.

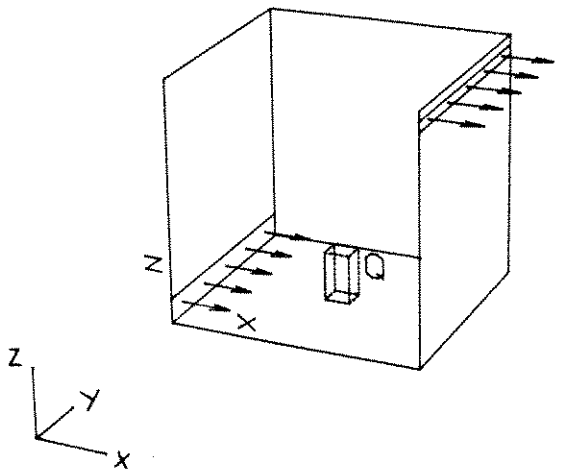

Figure 3.13. Configuration. The room is cubical with side-length L (=0.5 m). xz-plane y=L/2 is a symmetry plane. A heat source, Q, is introduced (uniformly distributed) in the region bounded by dotted lines in the middle of the room (0.48<x/L<0.52, 0.48<y/L<0.52, 0<z/L<0.22)

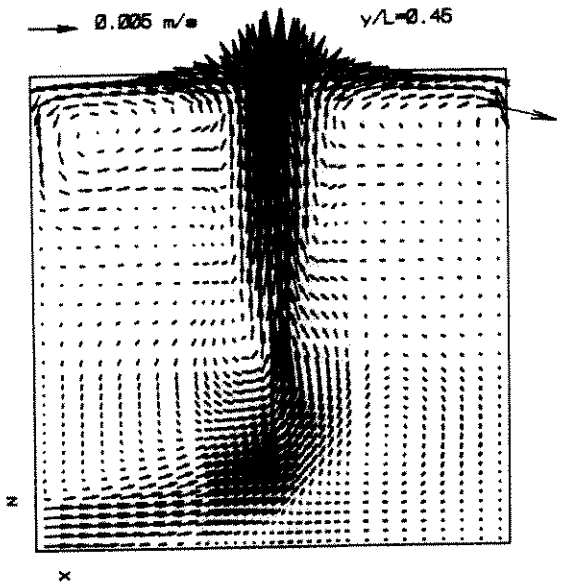

Figure 3.14. Calculated velocity vectors. xz-plane, y/L=0.45.

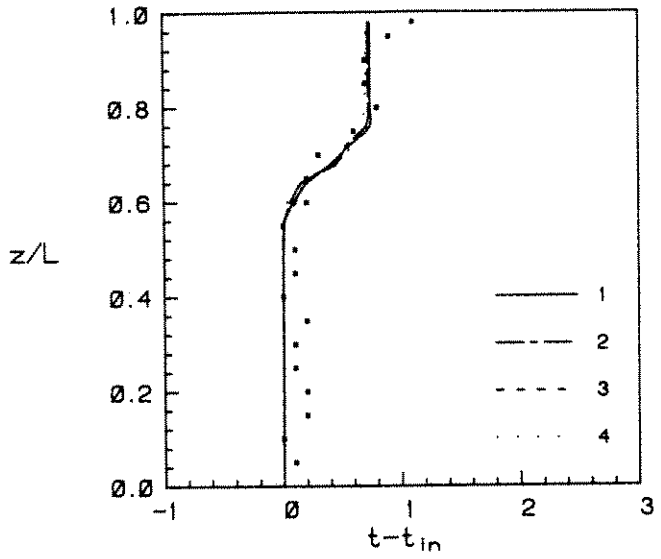

Figure 3.15. Temperature profiles along vertical lines. Line 1: x/L=0.1, y/L=0.1; line 2: x/L=0.9, y/L=0.1; line 3: x/L=0.1, y/L=0.4; line 4: x/L=0.9, y/L=0.4. Markers: experiments by Sandberg (1988).

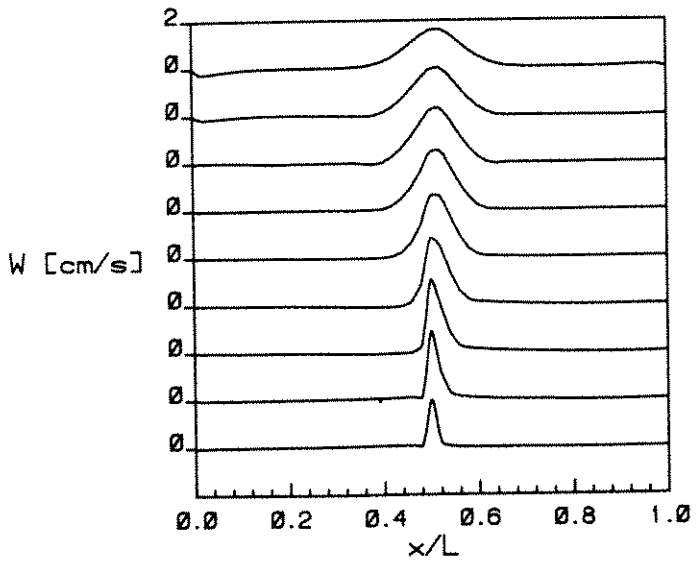

Figure 3.16. Calculated horizontal W-velocity profiles. xz-plane, y/L=0.5.

The calculated temperature profiles along four vertical lines are compared with experimental data in Fig. 3.15. It can be seen that the calculated results agree well with the experimental data; the experimental temperatures near the ceiling are, however, somewhat higher than the calculated ones. The reason for this may be that in the experiments warm water is trapped below the ceiling because the outlet is situated at some distance below the ceiling, or it may be that the ceiling is insufficiently insulated.

Horizontal W-velocities and temperature profiles for the planes x/L = 0.5 and y/L = 0.5 are presented in Figs. 3.16-3.17. Outside the plume, it is striking how constant both the W-velocity (which is close to zero) and the temperature are. The flow is very stratified outside the plume, and moves horizontally along the iso-thermals.

A parameter which is of great interest to an engineer who is designing a displacement flow system is the flow rate in the plume; when this parameter is known the value of the z_{front} is easily obtained ($z=z_{front}$ where $\dot{V}_{plume}=\dot{V}_{in}$). The flow rate in the plume as a function of the vertical coordinate, z, is shown in Fig. 3.18. The flow rate in the plume as a function of z was calculated as

$$\dot{V}_{plume}(z)=\int_{\delta A(z)} W(x,y,z)dA,\ W(x,y,z)>rW_{max}(z)$$

The area of the plume, $\delta A(z)$, in the integral is thus defined as the region where the W-velocity at the z-level in question is larger than $rW_{max}(z)$ [$W_{max}(z)$ is the maximum W-velocity at level z]. The factor r was chosen as 0.05; an increase of r to 0.1 altered the calculated flow rate less than 5 percent. According to Chen and Rodi (1979) the flow rate in a plume varies as z^m where m = -5/3; the predicted flow rate gives m = -1.52 for $z/L<0.6$. For larger z the flow rate increases at a much lower rate, because the temperature difference between the plume and its surroundings (which is the driving potential for the plume) decreases.

From the flow rate in the plume the value of the z_{front} is, as mentioned above, easily calculated. The predicted value $z_{front}/L=0.68$ agrees well with the experimental value $z_{front}/L=0.7$.

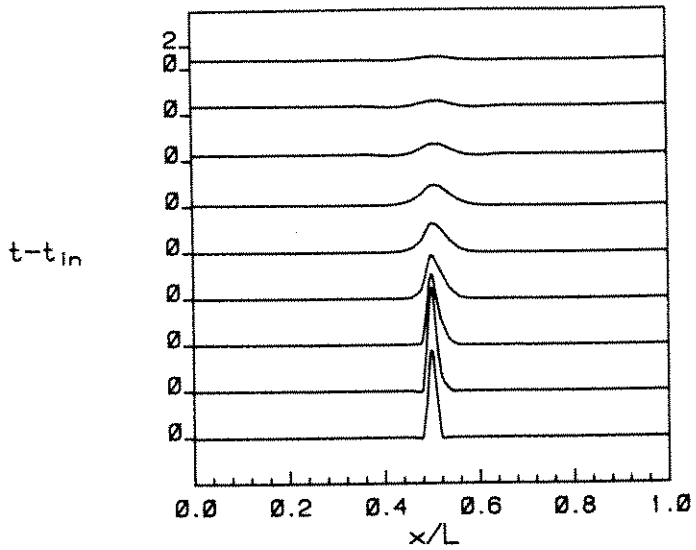

Figure 3.17. Calculated horizontal temperature profiles. xz-plane, y/L=0.5.

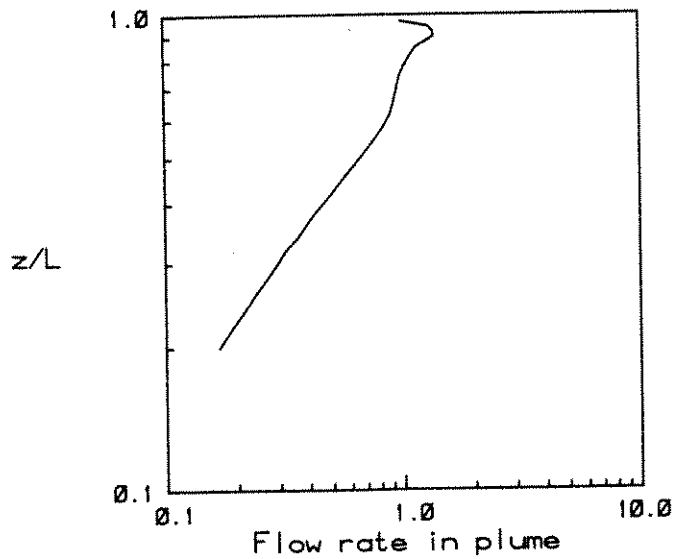

Figure 3.18. Calculated flow rate in the plume scaled with the total ventilation flow rate.

3.5 Paper VI

Turbulent flow, driven or affected by buoyancy, is an important type of flow which arises in many engineering applications. When calculating the flow in a ventilated room, for example, where the velocities are very small, it is very important that buoyancy effects are correctly accounted for. The heat transfer at walls is, in some cases (see Paper V), essential for the performance of the ventilation system. Near heating or cooling walls the flow can be strongly affected by buoyancy, and the viscous effects are usually large. This means that conventional wall functions, which are based on the use of local equilibrium logarithmic velocity and temperature assumptions, are not applicable.

In the present study the flow in a tall two-dimensional cavity of 5:1 aspect ratio with Rayleigh number of $4 \cdot 10^{10}$ (Cheesewright, 1988) is calculated using finite volume methods. The results obtained are compared with experimental data from Cheesewright et al. (1986).

The development of low Reynolds number turbulence models has, so far, been aimed at predicting low Reynolds number flows near walls. It is also very important to be able to predict low Reynolds number flow in free recirculating flows. In ventilated rooms, for example, the velocities are very small, and it is possible that the flow is not fully turbulent; the flow can also relaminarize owing to buoyancy effects.

As a first step towards a turbulence model able to predict this type of flow a modified form of a low Reynolds number k-ϵ model is developed. No near-wall terms are added to the equations in this model, and the damping equations include no irrelevant distance from the walls. It is hoped that this model could be used to predict free low Reynolds number flows, where the viscous effects are not due to walls.

The CELS solver developed by Galpin and Raithby (1986), which solves the linearized u, v, p and t-equations simultaneously along a line of control volumes, is implemented. This solver is used together with Newton-Raphson linearization of the convective terms in the temperature equation.

The objects of the present study are:

i) to develop a modified form of a low Reynolds number k-ϵ model as described above, and which is consistent in its near-wall behaviour and allows simulation of the decay of grid turbulence;

ii) to test this model and the model by Lam and Bremhorst (1981) in a flow driven by natural convection, and to compare the predictions with experimental data in order to investigate how well the models predict this type of flow, and how well the models predict low Reynolds phenomena such as transition and relaminarization;

iii) to investigate how efficient the modified CELS solver is in turbulent flow.

The CELS solver was originally formulated for flows where the Boussinesque approximation (small density variations) for the gravitational term is valid; as this is not the case in the present study, the solver is extended to be able to handle large density variations. The gravitational term in the v-equation is rewritten so that

$$-g(\rho-\rho_{ref}) = \rho_{ref}\, g\beta(t-t_{ref}) - g(\rho-\rho_{ref}) - \rho_{ref}\, g\beta(t-t_{ref})$$

where the first term on the right-hand-side of the equation was used in the CELS formulation, and the two remaining terms were included in the constant source term.

This solution method is compared with SIMPLEC, and it is shown to be up to more than three times as fast as SIMPLEC.

The k and ϵ-equations can be written

$$\frac{\partial}{\partial\tau}(\rho k) + \frac{\partial}{\partial x_i}(\rho u_i k) = \frac{\partial}{\partial x_i}\left[\left(\mu + \frac{\mu_t}{\sigma_k}\right)\frac{\partial k}{\partial x_i}\right] + P_k - \rho\epsilon \qquad (3.7)$$

$$\frac{\partial}{\partial\tau}(\rho\epsilon) + \frac{\partial}{\partial x_i}(\rho u_i \epsilon) = \frac{\partial}{\partial x_i}\left[\left(\mu + \frac{\mu_t}{\sigma_\epsilon}\right)\frac{\partial\epsilon}{\partial x_i}\right] + \frac{\epsilon}{k}\left(f_1 c_{\epsilon 1} P_k - f_2 c_{\epsilon 2}\rho\epsilon\right) \qquad (3.8)$$

where

$x_1=x$, $x_2=y$

$$P_k = \mu_t\left(\frac{\partial u_i}{\partial x_j} + \frac{\partial u_j}{\partial x_i}\right)\frac{\partial u_i}{\partial x_j} - \frac{\mu_t\, g\beta}{f_1\sigma_t}\frac{\partial t}{\partial x_2},\quad \mu_t = f_\mu c_\mu \rho k^2/\epsilon$$

$$\sigma_k = 1,\ \sigma_\epsilon = 1.3,\ \sigma_t = 0.9,\ c_\mu = 0.09,\ c_{1\epsilon} = 1.44,\ c_{2\epsilon} = 1.92$$

Patel et al. (1986) have tested a number of low Reynolds number k-ε models. They concluded that the model of Jones and Launder (1972) [hereafter denoted JL] was best, and that the model by Lam and Bremhorst (1981) [hereafter denoted LB] also gave results in good agreement with experiments. In the test case chosen in the present study, there are, according to experiments, transition regions from laminar to turbulent flow (as well as relaminarization). Rodi and Scheurer (1985) have used the LB model for predicting the flow along turbine blades, and in this flow there is also a transition region, which the LB model was shown to predict well in agreement with experimental data. For these reasons the LB model has been chosen in the present study. The functions and the boundary conditions for the LB model are given below.

The LB model:

$f_\mu = [1 - \exp(-0.0165\, R_n)]^2(1+20.5/R_t)$, $f_1 = 1 + (0.05/f_\mu)^3$, $f_2 = 1 - \exp(-R_t^2)$, $R_t = \rho k^2/(\mu\epsilon)$, $R_n = \rho k^{1/2} n/\mu$ where n is the normal distance from the nearest wall, $k = \frac{\partial \epsilon}{\partial n} = 0$ at walls.

The present model

In the present model, as well as in the LB model, the physical (isotropic) dissipation is solved, and the same form of the f_1-function as in the LB model is chosen. The disadvantage of the LB model is that the f_μ-function includes the distance from the wall. Since the f_μ-function, according to Patel et al. (1986), is the most important damping function, f_μ is taken from the JL model, i.e.

$$f_\mu = \exp\left[-\frac{3.4}{(1+R_t/50)^2}\right]$$

The object of the f_1-function is to increase the production of ϵ near the wall in order to decrease the turbulent kinetic energy. Since the f_μ-function in the LB model damps the viscosity (and k) much more than f_μ in the JL model, the constant in the f_1-function (=0.05) has to be increased in order to increase ϵ so that the turbulent kinetic energy decreases. Values between 0.05 and 0.16 on the constant were tested, and the value 0.14 was found to be optimum.

There are three main requirements for the function f_2:

i) it should force the dissipation term in the ϵ-equation to vanish at the wall;

ii) in order to render the ϵ-equation consistent at the wall, $f_2 \sim n^2$ is necessary (Patel et al., 1986);

iii) the constant $c_{2\epsilon}$ is determined from the decay of isotropic grid turbulence, where $k \sim x^{-m}$, and m=1.25 for high Reynolds numbers; in the final stage the exponent changes to m=2.5, and the f_2-function must take this into account.

It may be noted that the f_2-function in the LB model meets only one of these requirements (it does go to zero at the wall). In the present model the form of the f_2-function is taken as

$$f_2 = [1 - 0.27 \exp(-R_t^2)] \cdot [1 - \exp(-R_n)]$$

which meets all three requirements.

The QUICK scheme developed by Leonard (1979) [see Appendix in Paper VI] was used when discretizing the convective terms in the u, v and t-equations; in the k and ϵ-equations the hybrid upwind/central differencing scheme (HDS) was used. The reasons why QUICK was not used in the k and ϵ-equations are two-fold: the k- and ϵ-equations are rather insensitive to the choice of differencing scheme since they are very source dominated (Leschziner, Rodi 1981); second, QUICK can produce unphysical over and under-shoots, which could give negative values of k and ϵ which, of course,

is unphysical, and, furthermore, normally rapidly leads to divergence in the iterative solution.

Below, the calculated results are compared with the experiments by Cheesewright et al. (1986). These experiments suffer from two problems: there is a considerable heat loss through the side walls, and, more important, there is a small heat loss through the (well insulated) top wall. Near the top wall the flow is exposed to a positive vertical temperature gradient, which acts to reduce the turbulent kinetic energy [see Eqs. (3.7-8)]; this should cause relaminarization (which occurs near the bottom wall). Due to the small heat loss through the top wall, the temperature gradient is reduced, and the expected relaminarization does not occur. This results in asymmetry of the flow in the experiments, and for this reason the comparison between calculations and experiments is concentrated to the mid-plane, where end effects should not be so large.

The heat loss through the side walls reduces the core temperature, which results in loss of the 'diagonal symmetry' (the flow in the upper right part of the cavity should be similar, or identical if temperature effects on density and laminar viscosity are not taken into account, to that in the lower left part of the cavity).

A grid with 56x56 interior nodes is used, and it is generated using the equation

$$x_m = x_{max} \{-0.5 \tanh[\alpha(2 \frac{m}{n} - 1)]/\tanh(-\alpha) + 0.5\}$$

with α=3.5.

The configuration is shown in Fig. 3.19. In Figs. 3.20-21 the velocity field is presented in the form of velocity vectors and contours of the stream function, Ψ. The flow consists of a large clockwise vortex, and, from the contours of the stream functions, it can be seen that there are two small clock-wise vortices near the mid-plane y/H=0.5. The calculated v-profiles are compared with experimental data in Fig. 3.22. It can be seen that the agreement between prediction and experiments is good in the left half of the cavity, and that the predictions using the two different turbulence models are close to one an other; the predictions with the LB model

appear, in the core region, to be slightly better than those obtained with the present model, but both predicted profiles are probably within the bounds of experimental uncertainty. The discrepancy between the predicted profiles and the experimental profile near the cold (right) wall is due to the aforementioned incomplete relaminarization at the top wall in the experiments.

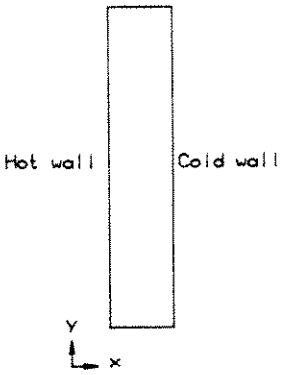

Figure 3.19. Configuration. t_H=80°C, t_C=34.2°C, H=2.5 m, L=0.5 m. Vertical walls are isothermal, and horizontal walls are adiabatic.

In Fig. 3.23 the predicted local heat transfer rates are compared with the experimental ones. First it should be noted that the predicted local heat transfer rates along the hot and cold walls are rather equal. The predicted heat transfer rate along the hot wall is slightly larger than that at the cold wall, due to that the laminar viscosity is higher at the hot wall. The experimental local heat transfer rates along the two walls, however, differ considerably from each other. This is due, as mentioned before, to the heat loss through the side walls which reduces the core temperature, and to the incomplete relaminarization near the top wall.

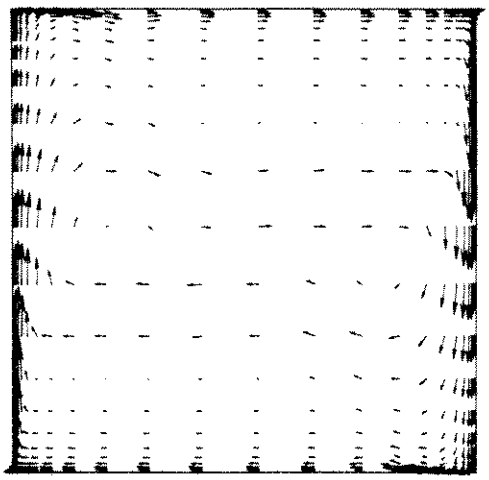

Figure 3.20. Predicted velocity vectors. Present model. Note change of scale in x-direction (see Fig. 3.19). Note that the velocity vectors only are drawn for every second control volume in the x and y-directions.

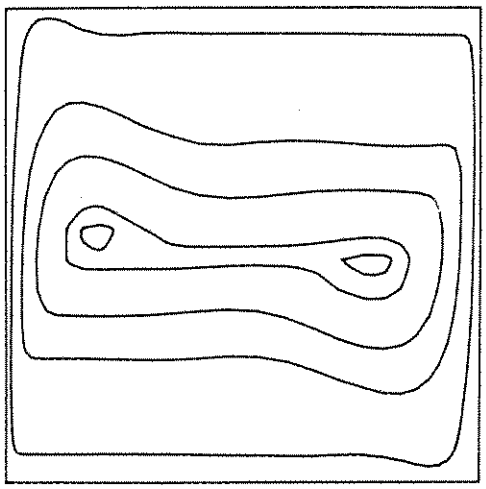

Figure 3.21. Predicted contours of the stream function. Note change of scale in x-direction (see Fig. 3.19). Present model.

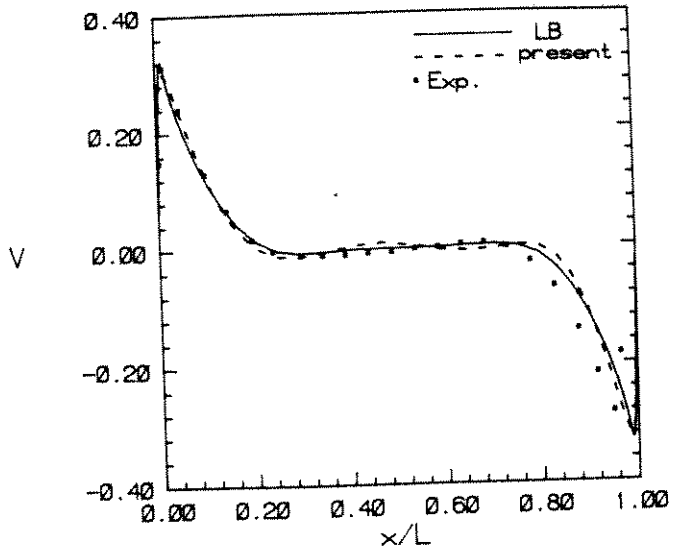

Figure 3.22. Predicted and experimental v-velocity profiles at y/H=0.5. Experiments by Cheesewright at al. (1986).

It can be seen in Fig. 3.23 that the predicted heat transfer rates at the vertical walls are larger with the present model than with the LB model; this is because the predicted turbulent viscosity close to the wall is larger with the present model than with the LB model (see Fig. 3.25). The predicted heat transfer rate with the present model agrees well with experimental data at the hot wall (see Fig. 3.23a), whereas the predicted values are higher than the experimental ones at the cold wall. The predicted heat transfer rates with the LB model are lower than experimental data at the hot wall, and vice versa at the cold wall. It is to be expected that, due to the heat losses through the side walls in the experiments, the experimental values should be too high at the hot wall, and too low at the cold wall. Accordingly, the heat transfer rates predicted with the present model should be too high; however, due to the problems in the experiments, no definite conclusion can be drawn if the predicted local heat transfer rates with the present model are better or worse than those obtained with the LB model.

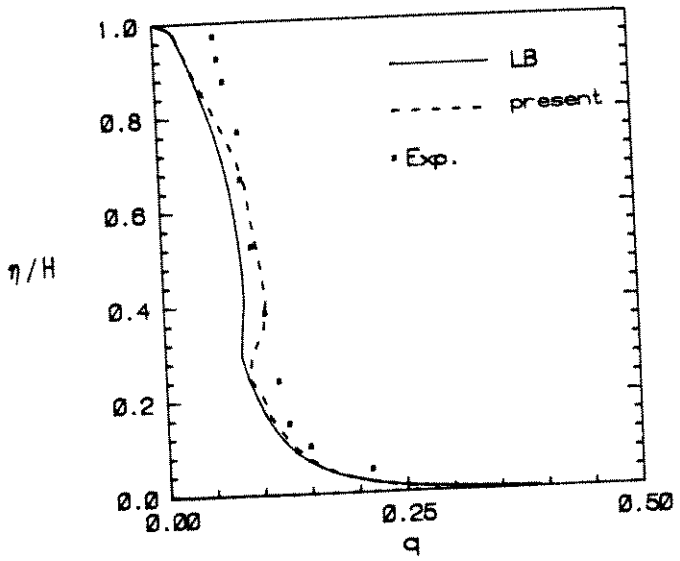

a)

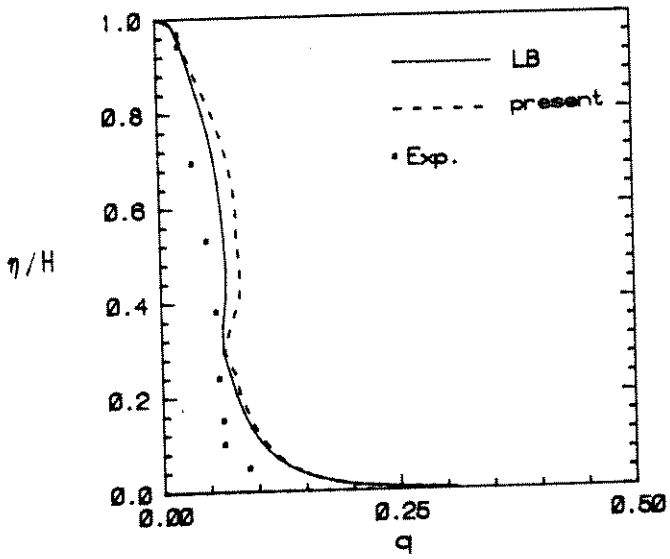

b)

Figure 3.23. Predicted and experimental local heat transfer rates at the vertical walls. Experiments by Cheesewright et al. (1986). a) Hot wall, b) cold wall.

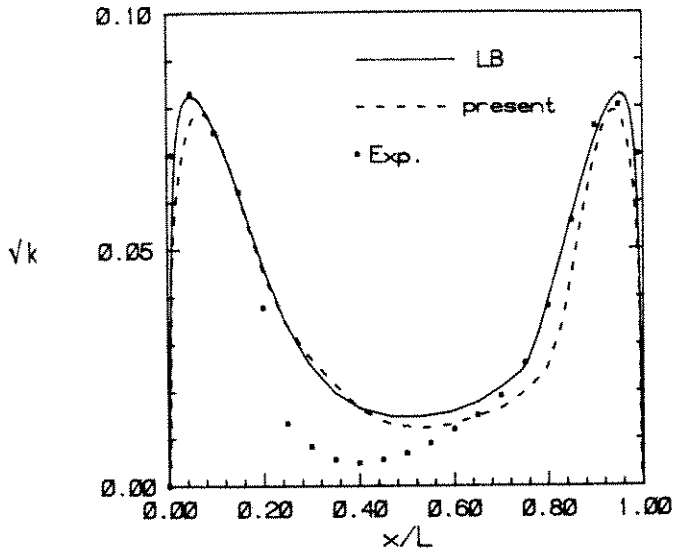

Figure 3.24. Predicted and experimental turbulent fluctuations, $\sqrt{k}$, at y/H=0.5. Experiments by Cheesewright <u>at al</u>. (1986).

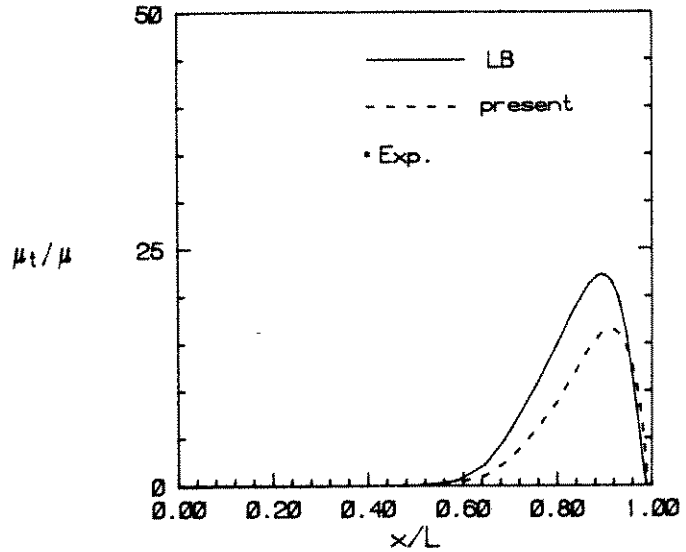

Figure 3.25. Predicted turbulent viscosity scaled with the laminar viscosity. a) y/H=0.1

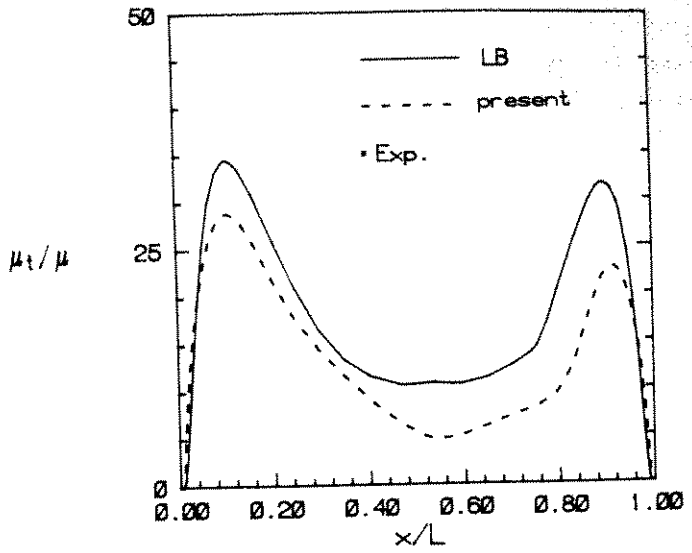

b)

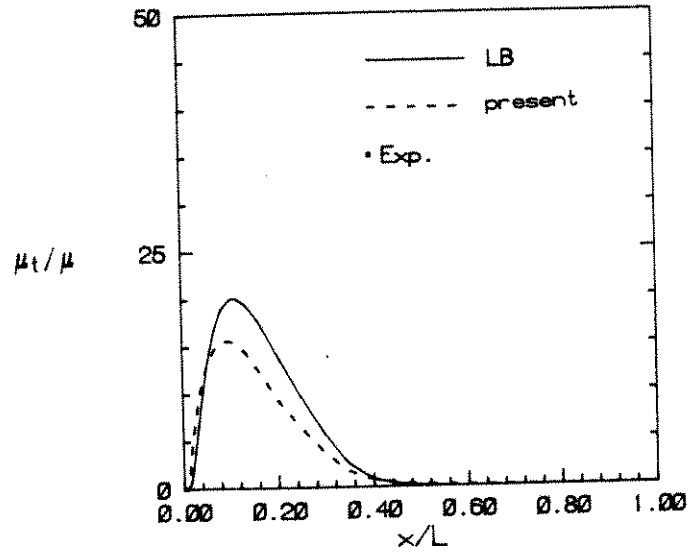

c)

Figure 3.25. Predicted turbulent viscosity scaled with the laminar viscosity. b) y/H=0.5, c) y/H=0.9.

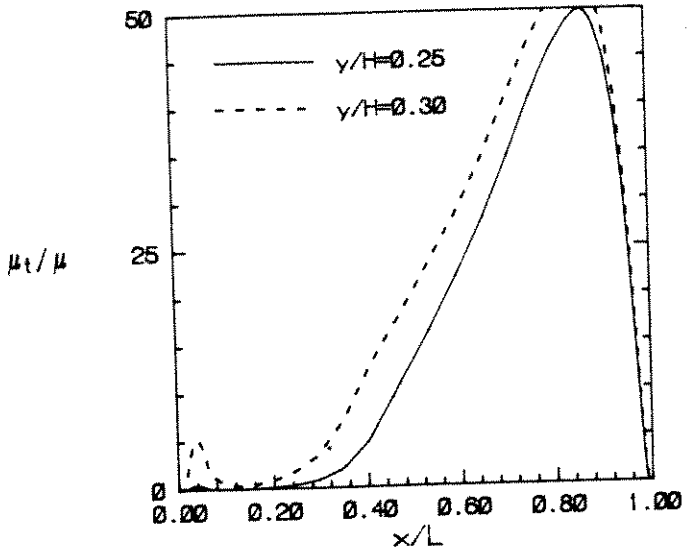

a)

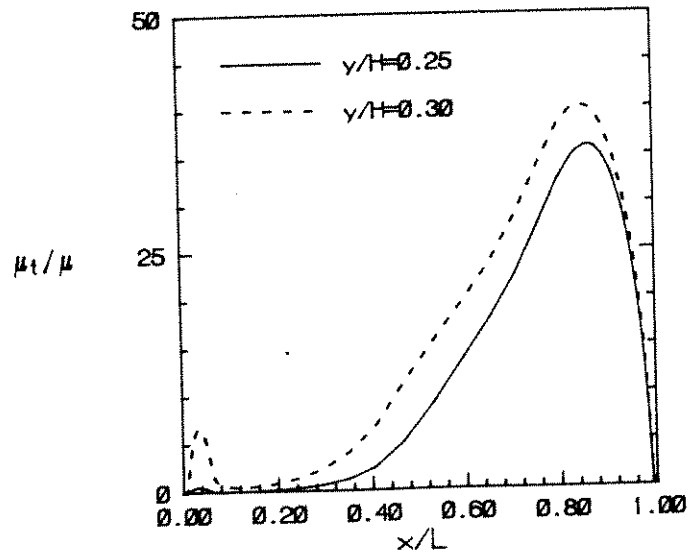

b)

Figure 3.26. Predicted turbulent viscosity at the hot wall scaled with the laminar viscosity. a) LB model. b) present model.

The present model predicts a sharp increase in q at $\eta/H \approx 0.25$-0.3. The model predicts transition here. There is also a small 'bump' in the curve for the LB model at $y/H \approx 0.3$ at the hot wall (see Fig. 3.23a), and this reflects a predicted transition region as well. This is in rather good (slightly better with the present model) agreement with the experiments by Cheesewright et al. (1986), where a transition region was found at approximately $\eta/H = 0.2$.

In Fig. 3.24 the predicted turbulent fluctuations are compared with experimental data, and both of the two turbulence models perform well. Even though the experimental $\sqrt{k}$-profile is rather asymmetrical, it can probably be concluded that the turbulence models predict too high a turbulence level in the core region.

The predicted turbulent viscosity using the present model is shown for various vertical levels in Fig. 3.25. Here it can be seen that the turbulent viscosity falls from a value of 15-20μ at the top of the hot wall (bottom of the cold wall) to zero at the top of the cold wall (bottom of the hot wall), showing the that the flow has, indeed, relaminarized at the top and bottom walls.

In Fig. 3.23 the predicted heat transfer rate indicate a transition region near $\eta/H \approx 0.3$. To further illustrate this, the predicted turbulent viscosity near the hot wall is shown in Fig. 3.26. Here it can be seen that at $y/H = 0.25$ the turbulent viscosity is just above zero, and that at $y/H = 0.3$ the turbulent viscosity has increased to approximately 5μ.

4. CONCLUDING REMARKS

When predicting fluid flow the question always arises: how accurate are the predictions? In this thesis all calculated results have been compared with experimental, analytical, or numerical data, and the agreement in most cases is good. The two-dimensional calculations presented in Papers I-IV, VI all agree well with data (experimental, analytical or numerical), and the three-dimensional isothermal calculations in Paper II also agree well with experiments. The predictions of the buoyancy driven flow in a rectangular cavity also agree well with experiments (Paper VI). There are, however, discrepancies between predictions and experimental data in the

three-dimensional buoyancy affected flows in Paper I, and for one case in Paper V. In these papers it is concluded that the discrepancies are explained by inaccuracies in the calculations and the experiments. One problem is that, for these cases, there is very little experimental data to compare with; in Paper I the local age and the temperature are measured in a few points, and in Paper V the temperature profile along one vertical line is measured. This is a problem in many full-scale experiments (as well as in the water box model in Paper V): the velocities are too low to be measured, and it is necessary to rely on temperature and concentration data. When predictions and experiments do not agree, it is very hard to tell why.

The possible inaccuracies in the predictions are well-known: grid dependent solutions, deficiencies in the turbulence model and the wall functions, and numerical diffusion due to the use of hybrid upwind/central differences. The author does not claim the solutions to be fully grid independent, but finds it unlikely that grid refinements would change the calculated results very much, and, indeed, some grid refinements were carried out in Papers I and V. The k-ϵ model of turbulence is also probably sufficiently accurate for this type of flow (it performs very well in the buoyancy driven flow in Paper VI). Nor is numerical diffusion believed to be a major source of error; firstly, because the same difference scheme was used in the isothermal calculations with good results, and, secondly, because the author has compared this scheme with other, more accurate schemes [QUICK by Leonard (1979), and skew-upwind differencing by Raithby (1976)] in flows in ventilated rooms (see Davidson, 1988; Davidson and Fontaine, 1989), and found that these more accurate schemes did not perform better than the hybrid upwind/central difference scheme. The author believes that, as far as inaccuracies in the predictions are concerned, the weakest point is the wall functions in estimating the heat transfer at the walls. The temperature field in a full-scale room (where the velocities are very low) is very important, as the flow is very stratified and move along the horizontal iso-thermals. The wall functions (or, rather, the boundary conditions) are more important for the temperature than for the velocities - at least in ventilated rooms - because the latter are mostly driven by pressure or gravity. The author suggests that either more sophisticated wall functions, or a low Reynolds number turbulence model should be used; the latter choice means that many more grid lines have to be located near the walls.

The inaccuracies in the predictions were discussed above, but, as mentioned in the beginning of this section, there are also inaccuracies in the experiments. The full-scale experiments are very sensitive to disturbances, such as a small change in the inlet conditions, a change of the wall temperatures so that the heat transfer through the wall is altered, etc. This can lead to that the stable stratification, which exist in the predictions, is disturbed and destroyed in the experiments.

REFERENCES

Aris, R., Vectors, Tensors and the Basic Equations of Fluid Mechanics, Prentice-Hall Inc., Englewood Cliffs, N.J. (1962).

Bobyleva, L.M., Zilitinkevich, S.S., and Laikhtman, D.L., "Turbulent Regime in a Thermally Stratified Planetary Atmospheric Boundary Layer", International Colloquium on the Microstructure of the Atmosphere and the Effect of Turbulence on Radiowave Propagation, Moscow (1965).

Cheesewright, R., King, K.J and Ziai, S., "Experimental Data for the Validation of Computer Codes for the Prediction of Two-Dimensional Buoyant Cavity Flows", in "Significant Questions in Buoyance Affected Enclosure or Cavity Flows", HTD-60, p. 75, ASME Winter Annual Meeting, Anaheim (1986).

Cheesewright, R., Private communication, Department of Mechanical Engineering, Queen Mary College, London (1988).

Chen, C.J. and Rodi, W., "Turbulent Buoyant Jets - a Review of Experimental Data", Pergamon Press (1979).

Davidson, L., "Turbulence Modeling and Calculation of Ventilation Parameters in Ventilated Rooms", Rept. 86/10, Thesis of Lic. of Engng., Dept. of Applied Thermodynamics and Fluid Mechanics, Chalmers University of Technology, Göteborg (1986).

Davidson, L., "Calculation of the Velocity and Concentration Fields in a Clean Room", Proc. Nordic Assoc. for Contaminant Control, Odense, Denmark (1988).

Davidson, L. and Olsson, E., "A Numerical Investigation of the Local Age and the Local Purging Flow Rate in Two-Dimensional Rooms", Proc. Room Vent 87, International Conference on Air Distribution in Ventilated Spaces, Stockholm, Sweden (1987).

Davidson, L., "Calculation of the Turbulent Flow and the Local Age in a Non-Rectangular Room Using a Finite Volume Computer Code Written in General Non-Orthogonal Coordinates", to be presented at CLIMA 2000, Dubrovnik, August (1989).

Davidson, L. and Olsson, E., "A Numerical Investigation of the Local Age and the Local Purging Flow Rate in Two-Dimensional Rooms", Proc. Room Vent 87, International Conference on Air Distribution in Ventilated Spaces, Stockholm, Sweden (1987).

Davidson, L. and Hedberg, P., "FLUX2D: A Finite-Volume Computer Program Written in General Non-Orthogonal Coordinates for Calculation of Two-Dimensional Turbulent Flow", Rept. 88/1, Dept. of Applied Thermodynamics and Fluid Mechanics, Chalmers Univ. of Tech., Göteborg (1988).

Davidson, L. and Fontaine, J.R., "Calculation of the Flow in Ventilated Rooms Using Different Finite-Difference Schemes and Different Treatment of the Walls", to be presented at CLIMA 2000, Dubrovnik, August (1989).

Fontaine, J.R., Gardin, P., Soumoy, V. and Aubertin, G., "Criteria for the Evaluation of General Ventilation Systems: Numerical and Physical Simulations", Proc. 2nd Int. Symp. on Ventilation for Contaminant Control, London (1988)

Galphin, P.F., Raithby, G.D. and Van Doormaal, J.P. "Discussion of Upstream-Weighted Advection Approximations for Curved Grids", Numer. Heat Transfer, Vol. 9, p. 241 (1986).

Galpin, P.F. and Raithby, G.D., "Numerical Solution of Problems in Incompressible Fluid Flow: Treatment of the Temperature-Velocity Coupling", Numer. Heat Transfer, Vol. 10, p. 105 (1986).

Gosman, A. D., Nie
Properties of Room
Vol 102 - 21[illegible]

Gosman, A. D., Nielsen, P. V., Restivo, A. and Whitelaw, J. H., "The Flow Properties of Rooms With Small Ventilation Openings", ASME J. Fluid Engng., Vol. 102, p. 316 (1980).

Hanel, B., "Methoden zur Vorausbestimmungen von Strömungsvorgängen in klimatisierten Räumen", PhD thesis, Technical University of Dresden (1980).

Hanel, B., Köthnig, "Methoden zur Vorausbestimmung von Strömungsvorgängen in klimatisierten Räumen", Luft- und Kältetechnik, Vol. 3, p. 136 (1983).

Hedberg, P.K., Rosten, R.I. and Spalding, D.B., "The PHOENICS Equations", CHAM TR/99, London (1988).

Hedberg, P.K., "Nondif: A Method to Avoid Numerical Diffusion and Over- and Under-Shoots", Proc. 6th Int. Conf. on Numerical Methods in Laminar and Turbulent Flow, Swansea (1989).

Hjerthager,B. H., "Flow, Heat Transfer and Combustion in Three-Dimensional Rectangular Enclosures", Thesis, Trondheim, NTH (1979).

Holmberg, R., Larsson, M. and Sundkvist, S. G. (1975), "Calculation of Velocity Distribution in a Ventilated Room", (in Swedish), VVS, No. 5, p. 59 (1975).

Jones, W.P. and Launder, B.E., "The Prediction of Laminarization With a Two-Equation Model of Turbulence", Int. J. Mass Heat Transfer, Vol. 15, p. 301 (1972).

Karki, K.C., "A Calculation Procedure for Viscous Flows at All Speeds in Complex Geometries", PhD thesis, University of Minnesota (1986).

Karki, K.C. and Patankar, S.V., "Calculation Procedure for Viscous Incompressible Flows in Complex Geometries", Numer. Heat Transfer, Vol. 14, p. 295 (1988a)

Karki, K.C. and Patankar, S.V., "Solution of some Two-Dimensional Incompressible Flow Problems Using a Curvilinear Coordinate System Based Calculation Procedure", Numer. Heat Transfer, Vol. 14, p. 309 (1988b)

Lam, C.K.G. and Bremhorst, K.A., "A Modified Form of the k-ε Model for Predicting Wall Turbulence", ASME J. Fluid Engng., Vol. 103, p. 456 (1981).

Larsson, M., "Predictions of Buoyancy Influenced Flow in Ventilated Industrial Halls", Proc. Heat Transfer in Buildings, Dubrovnik (1977).

Launder, B.E. and Rodi, W., "The Turbulent Wall Jet", Prog. Aerospace Sci., Vol. 19, p. 81 (1981).

Leonard, B.P., "A Stable and Accurate Convective Modeling Based on Quadratic Upstream Interpolation", Comp. Meth. Appl. Mech. Engng., Vol. 19, p. 59 (1979).

Leschziner, M. A. and Rodi, W., "Calculation of Annular and Twin Parallel Jets Using Various Discretization Schemes and Turbulence-Model Variations", ASME J. Fluid Engng., Vol. 103, p. 352 (1981).

Malin, M.R., Rosten, H.I., Tatchell and Spalding, D.B., "Application of PHOENICS to Flow Around Ship's Hulls", Second Int. Symp. on Ship Viscous Resistance, Gothenburg (1985).

Nielsen, P. V., "Berechnung der Luftbewegung in einem zwangsbelufteten Raum", Gesundheitsingenieur 94, Heft 10, pp. 299 (1973).

Nielsen, P. V., Restivo, A. and Whitelaw, J. H. (1979), "Bouyancy Affected Flows in Ventilated Rooms", Num. Heat Transfer, Vol. 2, p. 115,

Patankar, S. V., "Numerical Heat Transfer and Fluid Flow", McGraw-Hill, New York (1980).

Patel, V.C., Rodi, W. and Scheurer, G., "Turbulence Models for Near-Wall and Low Reynolds Number Flows: A Review", AIAA J., Vol. 23, No. 9, p. 1308 (1986)

Raithby, G.D., "Skew-Upwind Differencing Schemes for Problems Involving Fluid Flow", Comp. Meth. Appl. Mech. Engng., Vol. 9, p. 153 (1976).

Rodi, W., "Turbulence Models and Their Application in Hydraulics", International Association of Hydraulic Research, Monograph, Delft, The Netherlands (1980).

Rodi, W. and Scheuerer, G., "Calculation of Heat Transfer to Convection-Cooled Gas Turbine Blades", J. Engng. Gas Turb. and Power, Vol. 107, p. 620 (1985).

Sandberg, M., "What is ventilation efficiency?", Bldng Environ. Vol. 16, p. 123 (1981).

Sandberg, M., TM 279 (in Swedish), Dept. of Heating and Ventilation, Royal Institut of Tech., Stockholm (1984).

Sandberg, M., Private communication, National Swedish Institute for Building Research, Gävle, Sweden (1988).

Sandberg, M. and Sjöberg, M., "The Use of Moments for Assessing Air Quality", Bldng Eviron., Vol. 18, p. 181 (1983).

Sandberg, M. and Lindström, S., "A Model for Ventilation by Displacement", Proc. Room Vent 87, International Conference on Air Distribution in Ventilated Spaces, Stockholm, Sweden (1987).

Tailland, A. and Mathieu, J., "Jet Parétal", J. Mécanique, Vol. 6, p. 103 (1967).

Van Doormaal, J.P. and Raithby, G.D., "Enhancements of the SIMPLE Method for Predicting Incompressible Fluid Flows", Numer. Heat Transfer, Vol. 7, p. 147 (1984).